Are marl-limestone alternations mainly driven by $CaCO_3$ variations at the astronomical timescale? New insights from extraterrestrial ^3He

P.-H. Blard[1,2], B. Suchéras-Marx[3], G. Suan[4], B. Godet[1,3,4], J. Dutilleul[5], T. Mezine[3], T. Adatte[6]

1 - CRPG, CNRS, Université de Lorraine, 54500 Vandoeuvre-lès-Nancy, France
2 - Laboratoire de Glaciologie, Department of Geosciences, Environment, Society, ULB, Brussels, Belgique
3 - Aix Marseille Univ, CNRS, IRD, INRAE, Collège de France, CEREGE, 13400 Aix-en-Provence, France
4 - Université de Lyon 1, ENSL, CNRS, LGL-TPE, 69622, Villeurbanne, France
5 - GeoRessources, Université de Lorraine, CNRS, 54500 Vandoeuvre-lès-Nancy, France
6 - Institut des sciences de la Terre (ISTE), Faculté des géosciences et de l'environnement, Université de Lausanne, Lausanne, CH

This manuscript was submitted to Earth and Planetary Science Letters on January 5th 2023 for peer-review evaluation.

This is the non-peer reviewed version preprint submitted to EarthArXiv on January 6th 2023.

Words count:

7600 words + 9 figures

6 supplementary Tables:
https://ordar.otelo.univ-lorraine.fr/record?id=10.24396/ORDAR-108

Supp. Table 1 – Samples description
Supp. Table 2 – Major and trace elements of bulk sediments
Supp. Table 3 – Raw helium data
Supp. Table 4 – 3HeET derived sedimentation rates
Supp. Table 5 – Rock-Eval data
Supp. Table 6 – Nannofossil abundances

Keywords:
marl-limestone alternations; extraterrestrial ^3He; $CaCO_3$; Bajocian; Valanginian; orbital forcing

Abstract

Marl-limestone alternations are rhythmical inter-bedded deposits that commonly occur in many sedimentological environments. It is quite well established that these lithological variations originate from astronomically-driven climatic variations paced by the Milankovitch cycles of main periods 19, 23, 41, 100 and 405 ka. However, the sedimentological mechanisms involved are not clear: some models attribute these alternations to cyclic changes in the carbonate flux, while terrigenous siliciclastic input remained relatively constant. On the opposite, other models suggest that the carbonate flux was constant while the siliciclastic flux changed cyclically, or that both fluxes varied in antiphase. To disentangle these different scenarios, we collected marlstone and limestone samples from two sedimentary hemipelagic marl-limestone successions of Bajocian, Middle Jurassic (3 marl-limestone couplets over 3.4 m) and Valanginian, Lower Cretaceous (1 marl-limestone couplet over 0.9 m) from the Southern French Alps (Barles). We measured their concentrations in calcium carbonate, organic carbon, nannofossil, as well as in extraterrestrial ^{3}He ($^3He_{ET}$). Carbonate contents range from 45% in marls to 86% in limestones. Importantly, the measured $^3He_{ET}$ concentrations of all samples remained nearly constant in the siliciclastic fractions, within uncertainties (< 20%). Hence, our results indicate that, at the astronomical timescale, sedimentation rates were mainly controlled by large changes in the $CaCO_3$ net fluxes, leading to variable dilution of the terrigenous input. Nannofossil counting shows that pelagic $CaCO_3$ fluxes of coccolithophores are inversely correlated to the total carbonate content along the marl-limestone alternations and represent less than 7% of the total carbonate content. Hence, in this setting, these marl-limestone alternations were driven by fluctuations in micritic $CaCO_3$ supply from the nearby carbonate platform that variably diluted nannofossil and organic carbon particles. Finally, assuming a constant $^3He_{ET}$ flux of 100 pcc.cm^{-2}.Ma^{-1}, total $^3He_{ET}$-derived sedimentation rates range from 20 to 30 m/Ma in the marl strata, while they reach up to 80 to 100 m/Ma in the limestone layers. These sedimentation rates are broadly compatible with local average rates estimated for the whole Bajocian and Valanginian stages by biostratigraphy.

1 - Introduction

Limestone-marlstone alternations are well known rhythmic inter-bedded deposits that are commonly encountered in many different carbonate-rich marine settings of the Phanerozoic. These sedimentological patterns are omnipresent in continental shelf to deep-sea settings, with some of the oldest records dating back from the Early Paleozoic (Einsele et al, 1982). Although some studies suggested a diagenetic origin for these limestone-marls cycles (e.g. Munnecke et al. 2001; Nohl et al. 2021), the dominant hypothesis is that these alternations result from primary rhythmic sedimentation patterns driven by the so-called “orbital” climatic cycles (Gilbert 1895; Milankovitch 1941). This climatic variability is driven by the sinusoidal fluctuations of the Earth’s orbital parameters around the Sun, that control the climate through the seasonal repartition of insolation (e.g. Berger et al, 1993). These so-called Milankovitch cycles result from the combination of three main orbital cyclic parameters: eccentricity (405 and 100 ka periods), obliquity (41 ka), and precession (19 and 23 ka). However, the exact sedimentological processes transforming this orbital forcing into lithological alternation are still unclear. Several models exist (e.g. Einsele, 1982; Ricken, 1993): i) Some propose that the terrigenous siliciclastic flux remain constant during these cycles, while the carbonate input is variable and controlled by the orbitally driven climatic variations (e.g., (Van Os et al. 1994; Pittet and Mattioli 2002); ii) other models suggest that the carbonate input remains constant and that the siliciclastic flux is the main variable factor, through the control of climate on continental denudation (e.g., Van Os et al. 1994; Mount and Ward 1986); iii) Other models even suggest joined antiphase variations of both carbonate and terrigenous fluxes (Marcantonio et al. 2009; Woodard et al. 2011). These various models almost invariably used sedimentary cycle counts and spectral analyses of the rhythmic successions to build so-called astronomical age models and estimate the fluxes of carbonate and detrital components. Such age models are however inherently limited in temporal resolution (>20 ka) and are not able to measure relative changes in accumulation rates at the timescale of a single marl-limestone alternation. Moreover, depending on the analyzed setting, these approaches generally imply relatively subjective choices regarding cycle identification. Hence, given the coarse resolution and uncertainties of the astronomically-based fluxes, alternative methods are required to reconstruct sedimentation rates at ka-resolution and further constrain the processes controlling marl-limestone alternations.

Such ka-resolution age models can be achieved measuring the sedimentary abundance of particles of extraterrestrial origin. The Earth surface is indeed permanently bombarded by micrometeorites, known as interplanetary dust particles (IDPs), whose typical sizes are smaller than 100 μm. These IDPs bear significant amount of extraterrestrial ^{3}He (^{3}He$_{ET}$) and are sufficiently small to have remained below the helium diffusion temperature during their atmospheric entry (Mukhopadhyay and Farley 2006). These micrometeorites carry high amounts of ^{3}He$_{ET}$ accumulated by solar wind implantation and cosmic ray production. They bring to Earth a flux of ^{3}He$_{ET}$ that ranges between 10^3 and 10^4 at.cm^{-2}.yr^{-1} (McGee and Mukhopadhyay 2013), before being finally mixed in continental and marine sediments. Since

IDPs have a $^3He/^4He$ ratio that is several orders of magnitude higher than the one of the terrestrial rocks, it is possible to compute the proportion of helium carried by IDPs and the one carried by terrestrial silicates. The concentration of $^3He_{ET}$ measured in bulk sediment samples can hence be used as a proxy of past variations of extraterrestrial material flux over long term timescales (> 1 Ma) (Farley et al. 2006). This application requires the sedimentation rate to be independently known. Reversely, when the sedimentation rate is unknown, $^3He_{ET}$ concentrations in sediments may be used to determine the terrestrial sedimentation rate (e.g. (Marcantonio et al. 1995; 1996; Farley and Eltgroth 2003; Abell et al. 2021). This requires that the flux of $^3He_{ET}$ can be assumed constant, a hypothesis that is satisfied on < 100 ka timescales (Farley et al. 2012; McGee and Mukhopadhyay 2013). In this case, $^3He_{ET}$ is an efficient mean to determine sedimentation rates and we take here advantage of this method.

To improve our understanding of the origin of the marl-limestones alternations we present here new $^3He_{ET}$, $CaCO_3$, organic carbon and nannofossil contents of sedimentary samples collected along meter-scale limestone-marl alternations of a Bajocian (3.4 m – 23 samples) and a Valanginian (0.9 m – 6 samples) section from the French Southern Alps (Digne-les-Bains, France). We also performed Rock-Eval analysis to measure the total organic carbon (TOC; wt%) and assess the maximum temperature reached by the samples during their burial by orogenesis processes. We use these data to establish whether these alternations were controlled by changing detrital or carbonate fluxes (or a combination of both). The new $^3He_{ET}$ measurements yield sedimentation rates and changes in carbonate and organic carbon fluxes. The results unambiguously identify constant silici-clastic input, the variable carbonate net flux being the dominant processes controlling the studied lithological and geochemical patterns. This has important implications for our understanding of Mesozoic stratigraphy and biogeochemical feedbacks.

2- Geological settings and samples description

2-1 – The Mesozoic sedimentary terrains of the Barles half window

We sampled two carbonate-rich sedimentary successions of 3.4 and 0.9 m long, respectively belonging to the Bajocian and the Valanginian. Both are located in the foreland of the French Southern Alps, in the autochthonous Mesozoic cover of the Barles-Digne-les-Bains zone (Haccart et al. 1989) (Fig. 1). This Mesozoic sedimentary succession exposes different lithological facies: a few hundreds of meters of evaporites, restricted at the bottom of the pile, are topped by a pluri-kilometric thick succession of marine formations mainly composed of more or less regular alternations of limestone and marl beds (Fig. 1). Most of these marl-limestone rhythms were deposited in open epicontinental marine environments developed at the boarders of the Tethys Ocean and surrounded by a mosaic of emerged lands (Massif Central) and shallow water carbonate platforms (Provence in the South, Jura in the North), with important lateral variations in the bathymetry (Fig 2A and B).

Along the Bès river, the Barles section exposes a Mesozoic sedimentary cover of about 3000 m-thick from the Rhaetian (Upper Triassic) to the Albian (Lower Cretaceous) (Fig. 2C). Alternations of marl and limestone beds occur at different time scales and imply different controlling mechanisms. Over multi-million years timescale, the observed inter-stages limestone marl variations probably result from the combined effects of changes in tectonics, eustasy and climate (Graciansky et al. 1999). Over shorter timescales (<1 Myr), the marl-limestone lithological alternations in Southern France are often characterized by a clear rhythmicity that was probably paced by orbitally-driven climate changes (e.g. Martinez et al. 2015; Giraud et al. 1995; Sucheras-Marx et al. 2013).

This foreland zone of the external Alps has been affected by moderate to high intensity folding and faulting during the alpine orogenesis, that started at the Oligocene, 35 Ma ago (Ford et al. 2006). After its burial under the overlying pluri-kilometric sedimentary pile (3 km for the Valanginian, 4 km for the Bajocian; Figs. 1 and 2), the Barles folded window has later been buried under the ~3 km thick Digne thrust sheet 12 Ma ago (Fig. 1), before being exhumed around 6 Ma ago (Schwartz et al. 2017).

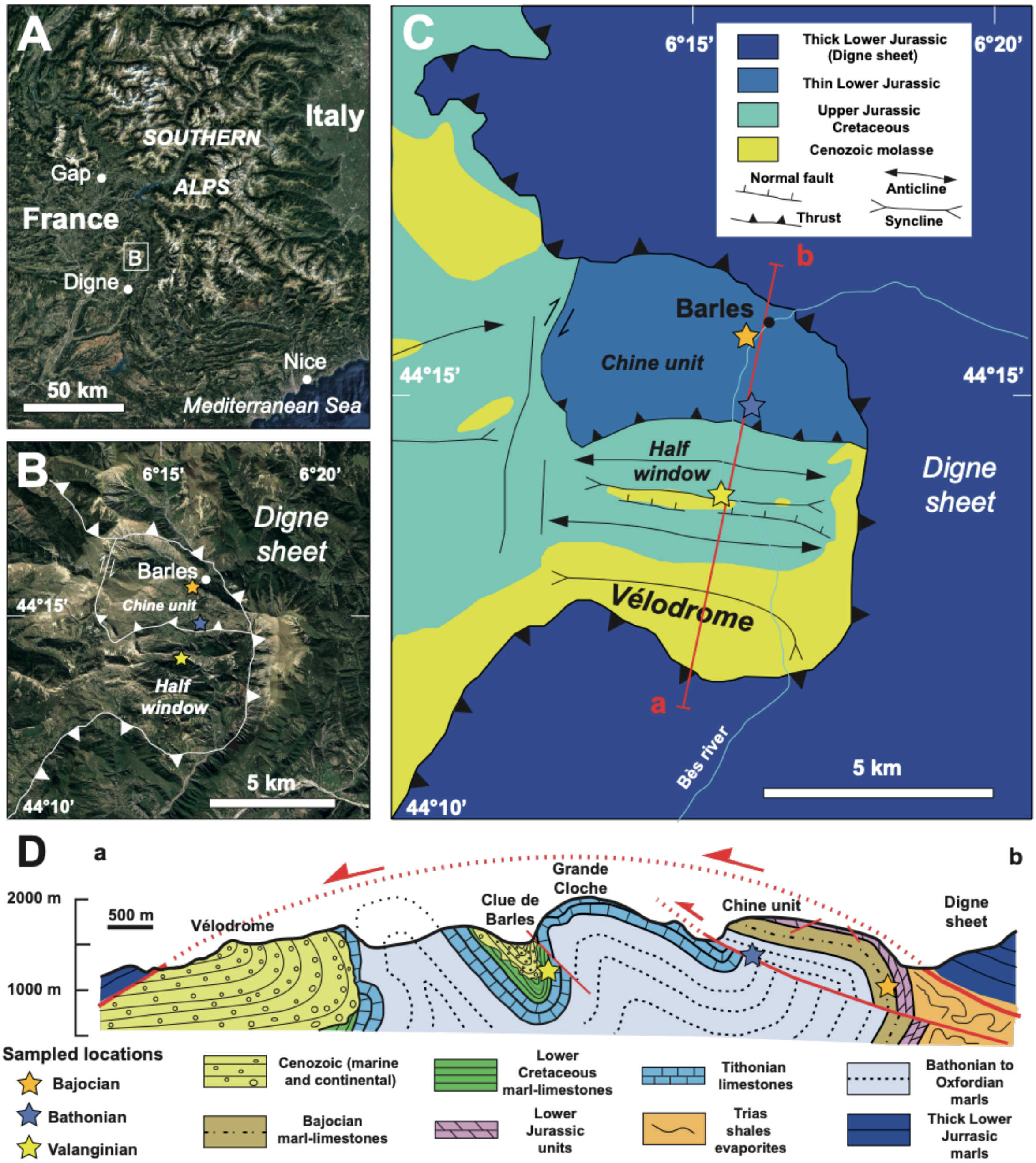

Figure 1 – A) Satellite picture of the Southern French Alps and localization of the studied area (square) © Google Earth, B) Satellite picture of the Barles half-window and the Digne sheet © Google Earth, C) Geological map of the studied area (modified from Agard and Lemoine 2005), D) North south cross-section of the Barles autochtonous half-window (modified from Agard and Lemoine 2005). Stars show the location of the sampled sections.

2.2 - Bajocian section (~170 Ma)

We collected 23 samples along a 3.38 m section of Bajocian age exposed on a continuous fresh outcrop in the northern bank of the Bès river (44.261036° N, 6.263431° E), the bedding dip is vertical with a strike of 110°N (Supp. Table 1, Figs. 1-3). The sampling site is located about 50 m above the base of the Bajocian formation, which has a total thickness of ~100 m at this location (Figs. 1 and 2). Our sampling covers three marl-limestone duplets (12 marl and 11 limestone samples). We removed the most altered surficial layers with a geological hammer, targeting fresh samples of ~500 g each. Samples positions were noted on the outcrop with a yellow mark and their relative positions in the vertical scale measured with a precision of about 2 cm (Fig. 3).

This Bajocian succession is characterized by an alternation of pluridecimetric thick calcareous beds and marly beds, with numerous *Zoophycos* trace fossils and *Stephanoceras* ammonites. The limestones have a mudstone facies. The detrital fraction is relatively rich in muscovite and has a silty-clay granulometry. The sedimentological characteristics indicate a depositional environment in an open marine platform located in the lower offshore bathymetric zone.

The timescale of the Bajocian stage remains rather poorly constrained relatively to other Mesozoic stages. Its biostratigraphic scheme based on ammonites (Cariou and Hantzpergue 1997) has been recently updated with calcareous nannofossil data (Ferreira et al. 2019). The GTS2020 (Gradstein et al. 2020) gives a duration of 2.73 Ma for the whole Bajocian stage. A cyclostratigraphic analysis ((Huang 2018) based on the dataset of (Ikeda, et al 2016)), indicate a total duration of 4 Ma for the two Bajocian-Bathonian stages, implying a duration of ~2 Ma for the Bajocian. However, a cyclostratigraphic study based on Chaudon-Norante section in the South Alpine basin suggested that the lower Bajocian stage may last at least 4 Ma (Sucheras-Marx et al. 2013), leading to a much longer estimate of 9.5 Ma for the whole Bajocian. These estimates bracket the average sedimentation rate between 10 and 50 m/Ma for the Bajocian section sampled at Barles (37 m/Ma using the 2.73 Ma duration of the GTS2020 timescale).

We also collected a single sample in the Bathonian-Oxfordian succession exposed near Saint Clément (44.245449°N, 6.267806°E), which is a >500 m thick, homogeneous unit of dark marls ("*Terres Noires*") deposited in ~8 Ma (Fig. 2), corresponding to a mean sedimentation rate of at least 60 m/Ma.

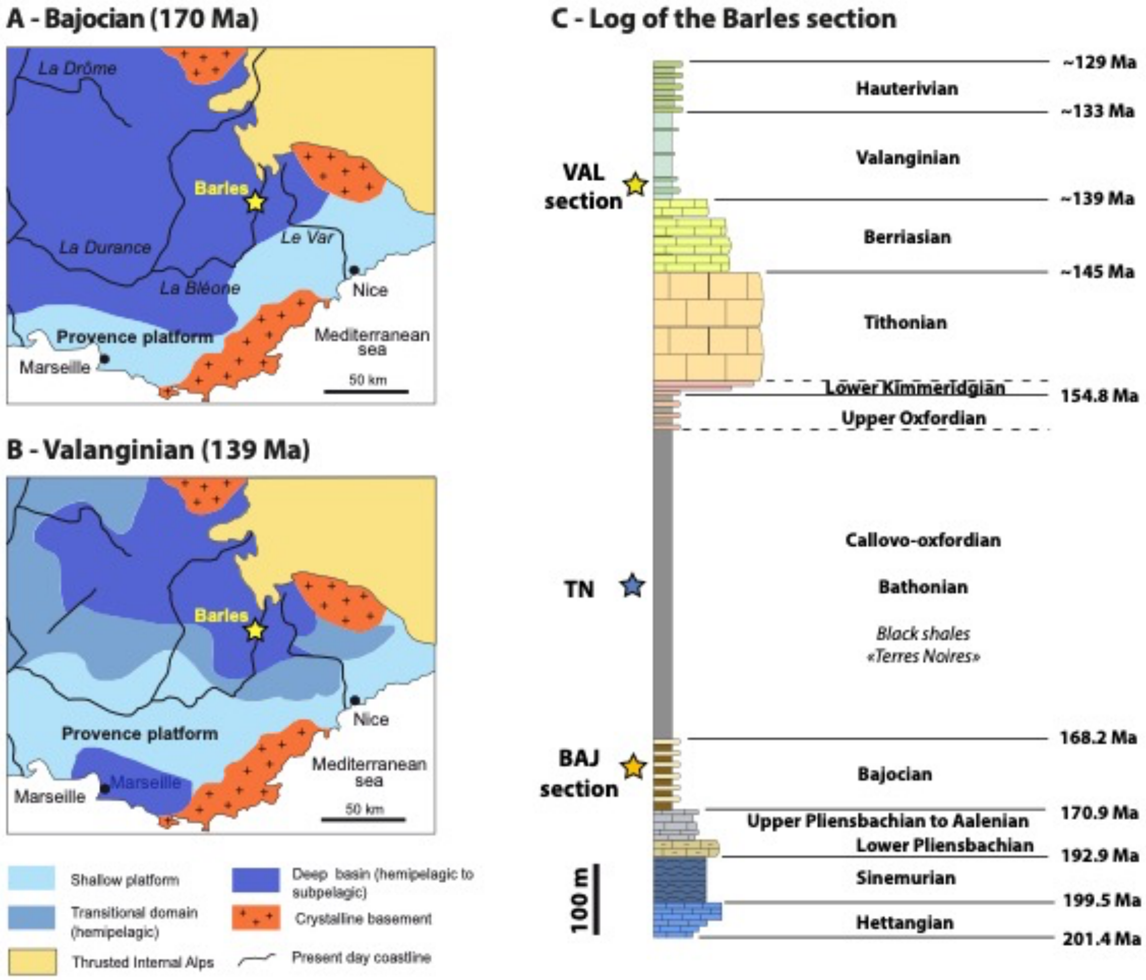

Figure 2 – A and B) Paleogeographic maps of the Southern French Alps during the Bajocian and Valanginian (modified from (Charbonnier et al. 2016) and (Olivero 2003)) - C) General log of the Barles half-window sedimentary cover (weathering profile). Stars show the position of the three sampled sections.

A - Bajocian section

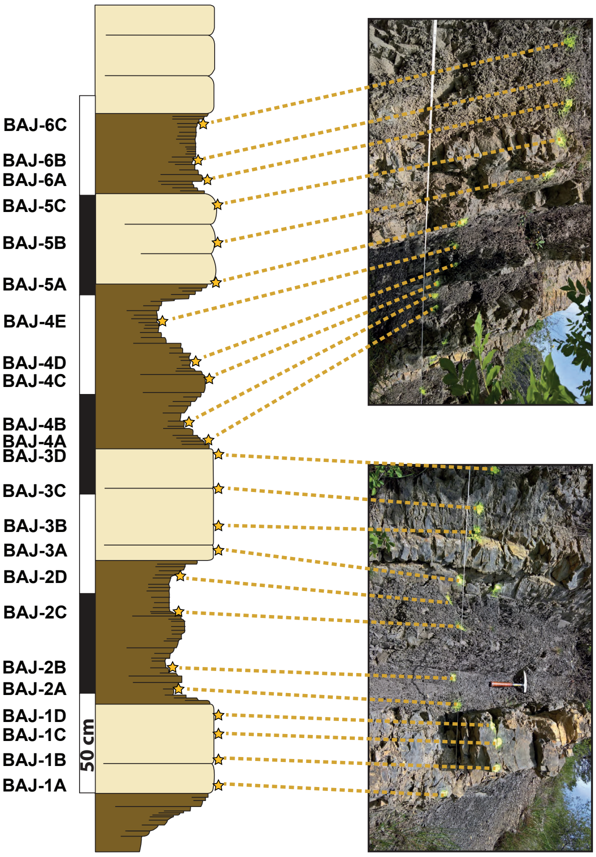

B - Valanginian section

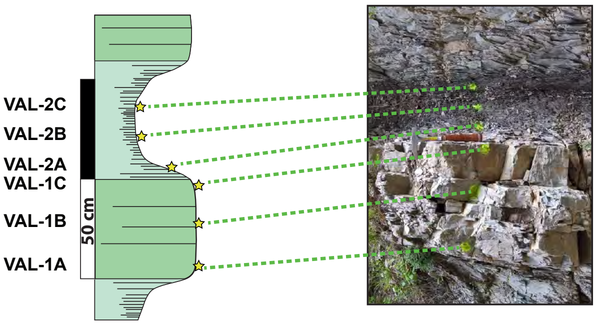

Figure 3 – Sedimentological log and picture of the A) Bajocian and B) Valanginian sampled sections. Stars show the positions of the samples.

2.3 - Valanginian section (~139 Ma)

We collected 6 samples along a 0.88 m succession of Valanginian age, in a fresh outcrop of a gulley on the right bank of a small tributary of the Bès river, at the southern edge of the

Clue de Barles (44.231113°N, 6.256626°E), where the bedding dip is vertical with a strike of 95°N (Supp. Table 1; Figs. 1-3). The sampled sections belong to the lowest part of the Valanginian, ~20 m above the top of the Berriasian formation. This section is characterized by submetric alternations of limestones and marls (Figs. 2 and 3). The 6 samples cover a single marl-limestone duplet (3 marl and 3 limestone samples). These limestones have a fine micritic facies, with no visible macrofossils, and the limestone-marl transition is very progressive. We targeted fresh samples of ~200 g each with a geological hammer. Sample positions were noted on the outcrop with a yellow mark and their relative positions in the vertical scale measured with a precision of about 2 cm (Fig. 3).

The total thickness of the Valanginian succession is 150 m at the sampling site. Assuming that the Valanginian is fully represented in this interval and its total duration is 5.1 Ma in GTS2020 (Martinez et al. 2013; Gradstein et al. 2020), the studied succession was deposited at an average sedimentation rate of 29 m.Ma^{-1}.

3 – Methods

3.1 - Samples preparation and dry bulk density measurement

We selected hand-size subsamples showing no visible fracture, no alteration crust, nor large clasts. Subsamples of ~50 g were then weighted, before being hold and weighed in water, in order to determine their volume by hydrostatic weighting, following the Archimedes' principle. Weights were then divided by volumes to compute the bulk densities.

3.2 - Major, trace elements and carbonate contents

The $CaCO_3$ content of the samples was estimated using three independent approaches: i) major elements (including Ca and C), and trace elements were analyzed at CRPG-SARM (Nancy) from 1 gram aliquots, with the standard protocol involving total alkaline fusion followed by ICP-OES, atomic spectroscopy and ICP-MS analyses (Carignan et al. 2001), ii) by measuring the residual weight of the non-carbonate fraction (NCF), obtained after 72 hours of 10% HCl digestion at room temperature, as part of the helium isotope measurements carried out on (see section 3.2.1) iii) by multiplying by 7.976 the mineral carbon contents (MinC) obtained during the Rock-Eval pyrolysis performed with 2 g aliquots (Jiang et al. 2017) (see section 3.5.).

3.3 - Helium isotopes analysis and calculations of sedimentation rates

3.3.1. Decarbonation

Subsamples of ~50 g were gently crushed and weighted. They were then dissolved in ~200 mL of 10% HCl during 72 hours, a duration sufficient to yield a total disappearance of any bubble. After centrifugation at 5000 rpm for 5 minutes, the supernatant was poured away. Then, remaining samples were rinsed three times in ~200 mL of deionized water. After each rinsing step, samples were centrifugated and the supernatant was again poured away. Although we paid a special attention to avoid unexpected loss of the remaining non-carbonate fraction, it is possible that a few % of the finest fraction of the sample were unintentionally lost during the rinsing steps. The decarbonated residues were then dried at 60°C for 48 hours and weighted to compute the proportion of the non-carbonate fraction relative to the initial weight.

3.3.2. Helium isotopes analysis

All helium isotope concentrations were measured at the CRPG Nancy noble gas facility with an upgraded SFT mass spectrometer (Mabry et al. 2013; Blard et al. 2015). ^{3}He and ^{4}He concentrations were measured in unseived decarbonated aliquots ranging in mass from 42 to 504 mg (weighting precision of 0.1 mg, 1σ) that were wrapped in tin foils before being loaded in the carrousel of a home designed high vacuum metal induction furnace (Zimmermann et al. 2018; Blard 2021). Helium was extracted by heating the samples at 1400°C during 20 min. Subsequent re-extraction were at blank levels, showing that this procedure was sufficient to release the totality of the helium from the samples. Associated ^{3}He and ^{4}He blanks were (7±7) × 10^3 atoms and (2.2±0.8) × 10^9 atoms, respectively. The blank correction represents less than 1% of the helium concentrations analyzed in these samples. After the sample heating, the extracted gas was cleaned in a metal purification line, using a succession of charcoals cooled in liquid nitrogen, foam getters and Ti-sponge, until the remaining pressure had reached less than 1 mbar. Finally, the remaining gas was focused in a cryosorber head cooled at 8 K, before being re-heated at 75 K and released in the SFT mass spectrometer for analysis (Blard et al. 2015; Blard 2021). The instrument sensitivity was calibrated using the HESJ helium standard (Matsuda et al. 2002), which has a certified ^{3}He/^{4}He ratio of 20.63 Ra (Ra = 1.384 × 10^{-6} being the atmospheric ^{3}He/^{4}He ratio). Long term external sensitivities of the SFT were (4.39±0.09) × 10^{18} cps/mol, and (7.87±0.02) × 10^{13} mV/mol for ^{3}He and ^{4}He, respectively. The analysis of a CRONUS-P pyroxene during the same analytical session, yielded ^{3}He and ^{4}He concentrations of $(4.88\pm0.06) \times 10^9$ at/g and $(3.55\pm0.06) \times 10^{13}$ at/g, in very good agreement with the calibrated value (Blard et al. 2015; Blard 2021).

3.3.3. Isotopic determination of the $^3He_{ET}$ component

In marine sediments, the helium isotopic budget is determined by a two-components isotopic mixing between the helium terrestrial silici-clastic endmember and the extraterrestrial endmember. Hence, we used the helium ratio (R_{sample}) and the total ^{3}He concentration ($^3He_{sample}$) measured in the bulk samples to compute the concentration of extraterrestrial ^{3}He ($^3He_{ET}$) (Marcantonio et al. 1995):

$$^3He_{ET} = \frac{1-\frac{R_{SC}}{R_{sample}}}{1-\frac{R_{SC}}{R_{ET}}} \times \ ^3He_{sample} \qquad (1)$$

, where $R_{SC} = (^3He/^4He)_{SC}$, and $R_{ET} = (^3He/^4He)_{ET}$ are the silici-clastic terrestrial and extraterrestrial isotopic ratios, respectively. Here we use a value of 0.01 R_a for R_{SC} and 300 Ra for R_{ET}. The value of R_{SC} is calculated considering that these isotopic endmembers equals the production ratio of nucleogenic ^{3}He and radiogenic ^{4}He, using the equations of Andrews and Kay (1982), Andrews (1985) and Blard (2021) and the major and trace elements measured in the samples, assuming a Li concentration of 75±25 ppm in the silici-clastic component (Teng et al. 2004). Since R_{SC} has shown variations in different materials (McGee and Mukhopadhyay 2013; Marcantonio et al. 1998), we consider here a significant relative uncertainty of 50% on R_{SC}, as well as R_{ET}, and propagate this uncertainty using the Taylor's formula on the calculation of $^3He_{ET}$ with equation (1).

Recent work showed that atmospheric helium may be absorbed on the surface of recently crushed silicates (Protin et al. 2016; Cox et al., 2021). However, given the granulometry of the analyzed samples (D_{50} from 5 to 15 μm, Supp. Table 1), the amplitude of this potential contamination is 1 to 2 orders of magnitude lower than the ^{4}He concentrations measured in these samples, implying that a potential contamination by atmospheric helium can be safely neglected.

3.3.4. $^3He_{ET}$ concentrations in sediments: a way to measure sedimentation rates

If the net flux of $^{3}He_{ET}$, F_{ET} (at. m^{-2}.Ma^{-1}) can be assumed constant over the timescale of interest, the concentrations of $^{3}He_{ET}$ measured in the non-carbonate fraction of sediments can be used to compute the mean terrigenous sedimentation rate, S_{SC} (m/Ma) (e.g. Farley 1995; Abell et al. 2021):

$$S_{SC} = \frac{F_{ET}}{\rho \times {}^{3}He_{ET}} \qquad (2)$$

, where ρ (g/m^3) is the bulk density of the analyzed sample. Here we used a mean $^{3}He_{ET}$ accumulation rate of 2.7×10^{13} at.m^{-2}.Ma^{-1} (100 pcc.cm^{-2}.Ma^{-1}), an average value based on the stack record of Farley et al. (2012) covering the 100-34 Ma period.

Then, knowing the non-carbonate fraction (NCF), the total sedimentation rate S_{Tot} (m/Ma) is obtained from:

$$S_{Tot} = \frac{S_{SC}}{NCF} \qquad (3)$$

With:

$$S_{Tot} = S_{SC} + S_{CaCO3} \qquad (4)$$

S_{CaCO3} (m/Ma) being the net calcium carbonate sedimentation rate.

3.4 - Laser granulometry

We analyzed the granulometric distribution of aliquots of ~100 mg of the non-carbonate fraction using the laser granulometer (Malverner Mastersizer 3000®) of the Laboratoire de Glaciologie of ULB (Université Libre de Bruxelles).

3.5 - TOC determination and rock-Eval pyrolysis

We measured total organic carbon (TOC, wt.%) content, mineral carbon (MinC, wt.%) content, hydrogen index (HI, mg HC/g TOC, HC=hydrocarbons), oxygen index (OI, mg CO_2/g

TOC), and T_{max} (°C) in powdered whole-rock sample using a Rock-Eval 6 (Espitalie et al., 1985; Behar et al., 2001) at the Institute of Earth Sciences of the University of Lausanne (ISTE–UNIL), Switzerland. Measurements were calibrated using the IFP160000 standard. T_{max} gives an estimate of the thermal maturation level of the organic matter (Espitalie et al., 1985; Peters 1986). Pyrograms were carefully checked and HI values were not interpreted for TOC $\leq$0.2 wt.%, and T_{max} values for $S_2 \leq 0.3$ mg HC/g to avoid misinterpretation of flat thermograms (Peters 1986).

3.6 - Calcareous nannofossil slide preparation and quantification

We applied a random-settling method for calcareous nannofossil slide preparation (derived from (Beaufort et al 2014; Beaufort 1991). After crushing with an agate mortar, 1 mg of powder (weighted with a 0.1 μg precision microscale) was mixed with 35 mL of water in a beaker and placed during a few seconds in an ultrasonic cleaner. Next, 40 mL of water was added in the beaker. 1 mL of this solution was pipetted in a dedicated decantation device, and this volume was finally completed by 2 mL of the same solution; the device being protected with a precisely weighed cover slide. The powder was left for decantation at least 4 h. Then, the water was cautiously aspirated out and the cover slide was oven-dried at 50°C overnight. The cover slide was weighed again and then glued on a slide with a Norland optical adhesive 74 glue which crystallized in a UV cage after 30 s under radiation.

The calcareous nannofossils were observed and counted using an optical microscope Leica DM6000 with a red filter (655 nm) under ×1000 magnification, a set of circular polarizers (one right and one left) and a right circular analyzer. Whole calcareous nannofossils (≥ 50% of the fossils) were counted in at least 50 fields of views. However, all identifiable calcareous nannofossils represented by both whole specimens and fragments were photographed with a Spot Flex Monochromatic 15.0 64 Mpx. The pictures were directly used to measure the mass of the calcareous nannofossils and the mass of the calcite within each field of view following the method of Beaufort et al. (2021) for calcite mass quantification. The total mass of calcareous nannofossil calcite was estimated using the ratio between the sum of the mass of the fields of view and the sum of the mass of all calcareous nannofossils observed (whole and fragments). The absolute abundance (AbAb) of calcareous nannofossil in nannofossils/g was calculated following:

$$AbAb = \frac{n}{fov} \times \frac{9216}{m_{sample} \times 10^{-3}} \qquad (5)$$

with *n* the number of calcareous nannofossil counted, *fov* the number of fields of view, 9216 the number of fields of view within a cover slide, m_{sample} the mass of powder on the cover slide in mg. The mass contribution to the bulk rock of calcareous nannofossils $CaCO_3$ ($CaCO_{3Nanno}$) in wt% was then computed as follow:

$$CaCO_{3\,Nanno} = \frac{sum\ of\ measured\ mass\ nannofossil}{sum\ of\ measured\ mass\ fov} \times CaCO_3 \qquad (6)$$

with $CaCO_3$ the proportion of calcium carbonate in the bulk rock (in wt%).

4 - Results

4.1 - Carbonate fraction, major trace elements, dry bulk density and granulometry

$CaCO_3$, dry bulk densities (DBD) and granulometry of the NCF fractions are provided in Supp. Table 1 while major, trace elements are available in Supp. Table 2. The $CaCO_3$ contents range from 45 wt.% in marls to 86 wt.% in limestones (Figs. 4 and 5). The three methods used to determine the carbonate contents yield dataset that are highly correlated (R^2>0.97). However, for several samples, the HCl dissolution method yields $CaCO_3$ contents that are up to 10 wt% higher than those obtained by the two other methods. This indicates possible loss of NCF during the rinsing steps, leading to overestimate of the actual $CaCO_3$ fraction. Hence, in the following, we only consider the $CaCO_3$ fraction measured at SARM. Since samples do not display evidence of biogenic silica nor secondary authigenic minerals (e.g. pyrite), we assume that the NCF content consists only of silici-clastic material.

DBD range between 2.41 and 2.64 g/cm^3 for Bajocian samples, and between 2.31 and 2.61 g/cm^3 for Valanginian samples. $CaCO_3$-richer samples generally have the highest DBD values. A similar range of DBD values and relationships with $CaCO_3$ were reported for lower Bajocian samples from the Chaudon-Norante section, Subalpine Basin, France (Sucheras-Marx et al. 2013).

Grain size distribution of the NCF measured by laser granulometry yield D_{50} (median value) ranging from 3.8 to 17.6 microns, with a mean value of 9.3 microns (Figs. 4 and 5). The silici-clastic fractions (NCF) of limestones are characterized by smaller grain sizes (D_{50} of 7.7

µm and 3.9 µm for the Bajocian and Valanginian sections, respectively) than those of the marls (D$_{50}$ of 12.4 µm and 8.5 µm for the Bajocian and Valanginian sections, respectively (Supp. Table 1). Grain size distributions are unimodal, mode and median being similar.

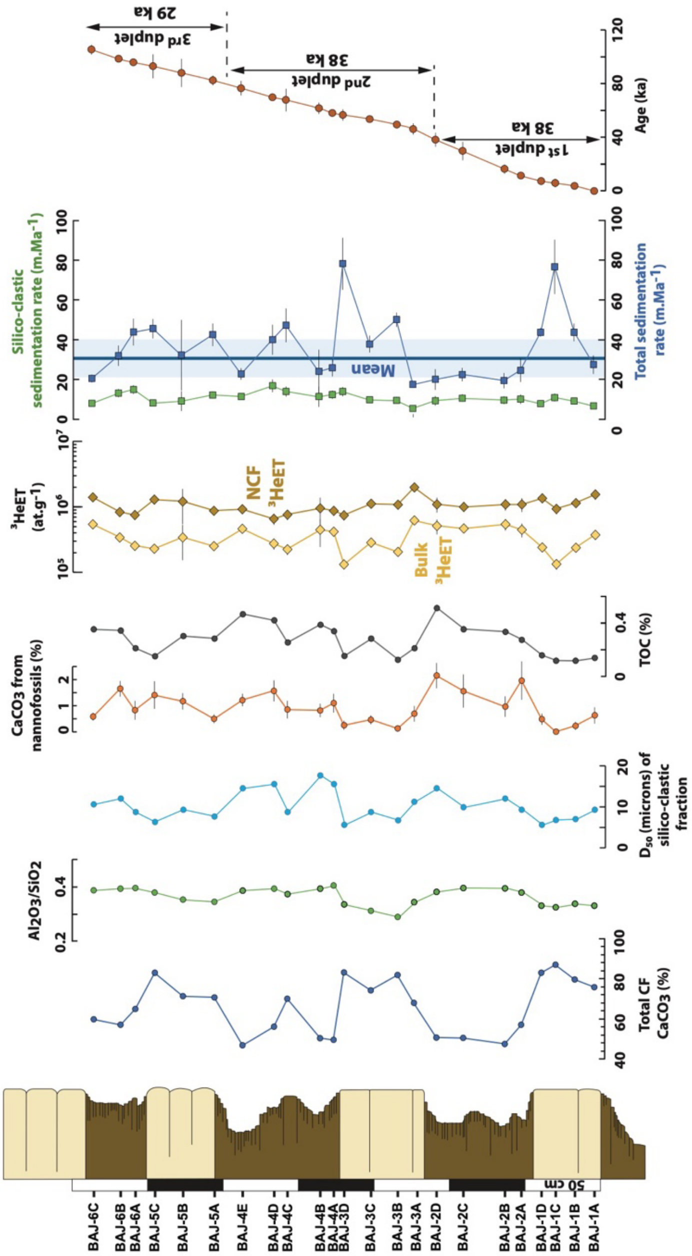

Figure 4 – Log of the Bajocian section with carbonate fraction, Al_2O_3/SiO_2 (proxy of clays/quartz), D$_{50}$ (µm) of silici-clastic fraction, $CaCO_3$ from nannofossils (wt %), Total Organic Carbon (%), $^3He_{ET}$ concentration (at/g) in the NCF fraction and in the bulk sediment, silici-clastic sedimentation rate, total sedimentation rate, mean accumulation rate, age model

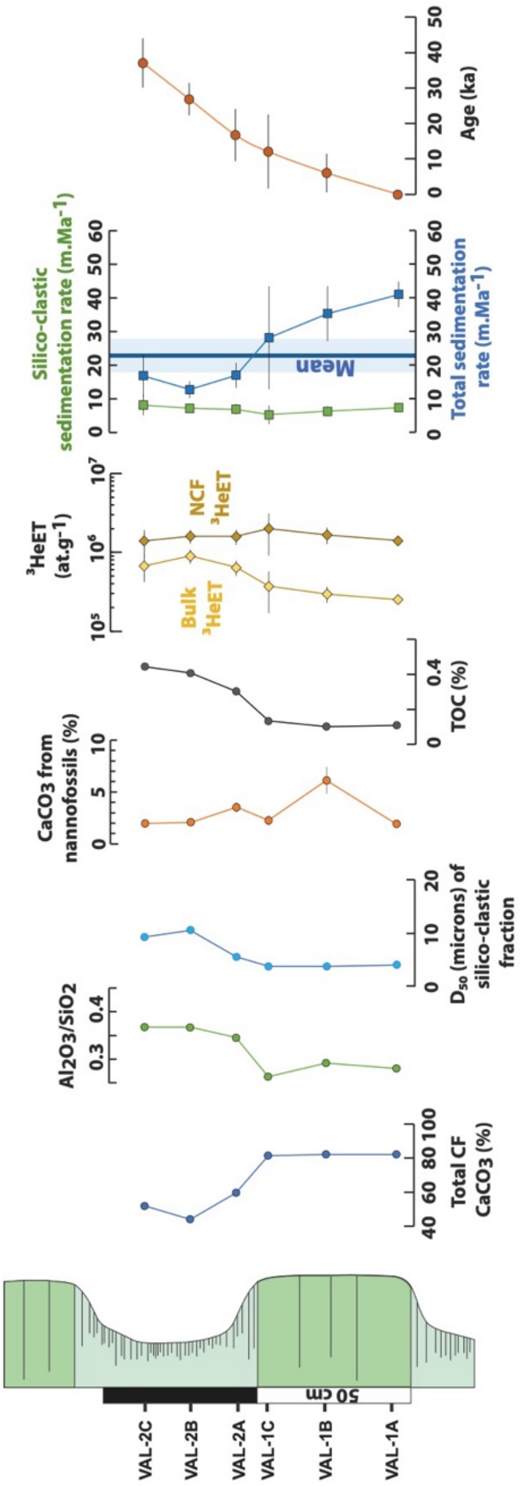

Figure 5 – Log of the Valanginian section with carbonate fraction, Al_2O_3/SiO_2 (proxy of clays/quartz), D_{50} (µm) of silici-clastic fraction, $CaCO_3$ from nannofossils (wt %), Total Organic Carbon (%), $^3He_{ET}$ concentration (at/g) in the NCF fraction and in the bulk

sediment, silici-clastic sedimentation rate, total sedimentation rate, mean accumulation rate, age model

4.2 - ^{3}He and ^{4}He concentrations

All helium results are presented in Supp. Table 3, with analytical uncertainties at the 1σ level. Bulk ^{3}He and ^{4}He concentrations measured by fusion range from $(0.80\pm0.23) \times 10^6$ to $(2.87\pm0.14) \times 10^6$ at/g and from $(0.51\pm0.01) \times10^{13}$ to $(2.03\pm0.03) \times 10^{13}$ at/g, respectively. Bulk (^{3}He/^{4}He) ratios range from 0.042±0.005 Ra to 0.222±0.018 Ra, values that are statistically above the value of the pure siliciclastic endmember R_{SC} (R_{SC} = 0.010±0.005 Ra) (Fig. 6). Computed $^3He_{ET}$ fractions using the two endmembers mixing assumption (Equation 1) range between 76 and 96%, the average value being 87% (Fig. 6). Associated relative uncertainties are anti-correlated with the proportion of $^3He_{ET}$ and range from 2 to 12% (1σ). Hence, even considering a 50% uncertainty on the crustal ^{3}He/^{4}He isotopic ratio (McGee and Mukhopadhyay 2013; Marcantonio et al. 1998), the proportion of $^3He_{ET}$ is high enough to ensure a statistically robust determination of the extraterrestrial excess, above the terrestrial ^{3}He background (Fig. 6).

^{4}He concentrations are positively correlated with the sample granulometry. Moreover, (U-Th)/^{4}He ages that are tentatively computed from the bulk U-Th and ^{4}He concentrations are younger than 1 Ma. Such ages are considerably lower than the depositional ages of these sedimentary rocks, and even than the age of 6 Ma estimated for the exhumation event that occurred after the emplacement of the Digne sheet (Schwartz et al. 2017). Since the granulometry (D_{50}) of the silici-clastic fraction is smaller than the α-ejection-implantation of 20 μm, it is highly probable that the radiogenic ^{4}He produced in these sedimentary samples has continuously escaped form these sediments.

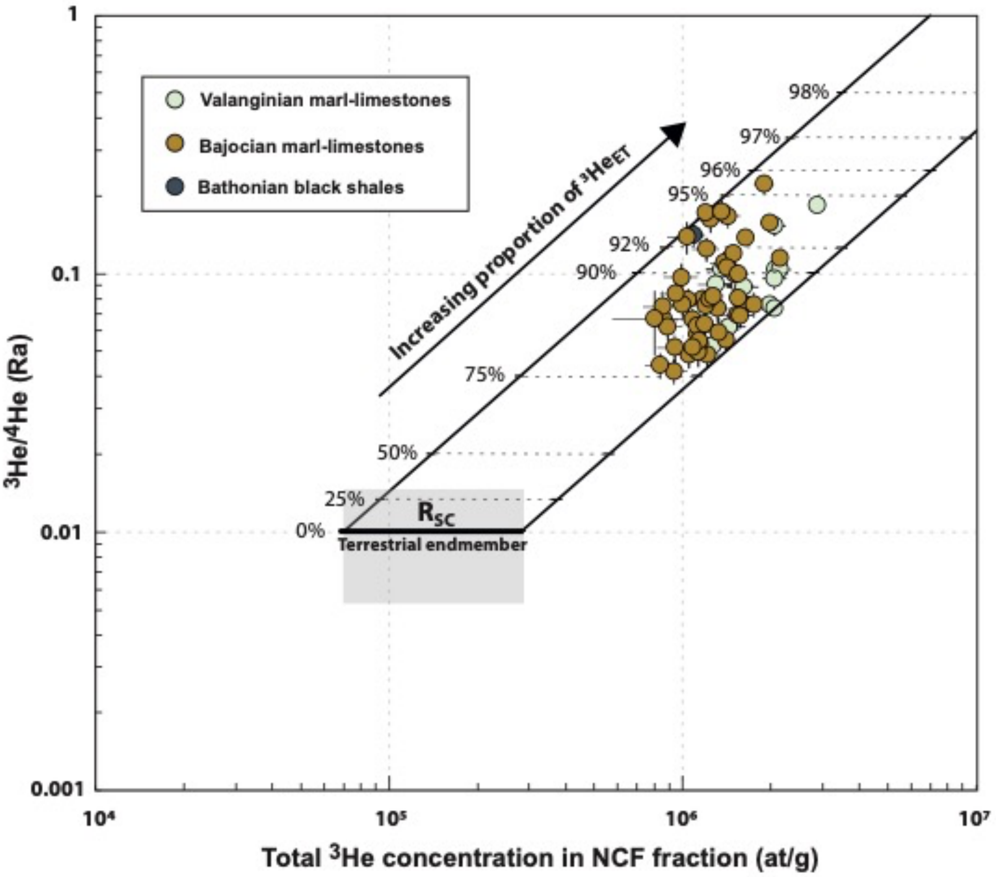

Figure 6 – Measured ^{3}He/^{4}He ratio (Ra) vs total ^{3}He concentrations (at/g) measured in the NCF fraction. Black lines show variable mixing between the terrestrial and the extraterrestrial helium endmembers, with ^{3}He/^{4}He isotopic ratios of 0.010±0.005 Ra and 300 Ra, respectively. Range of the terrestrial endmember (grey box) is defined considering the minimum and maximum ^{4}He concentrations measured in this dataset, and for R_{SC} a theoretical production $^3He_{nucleogenic}/^4He_{radiogenic}$ ratios of 0.01 Ra.

$^3He_{ET}$ concentrations in the silicate fraction range from (0.65±0.12) × 10^6 at/g (BAJ-4D) to (2.72±0.16) × 10^6 at/g (VAL-1C). Most of replicates of a same sample (n = 2 to 4) agree within 2σ uncertainties, indicating that the interaliquot variability is comparable with the analytical uncertainties. This suggests that the analyzed aliquots (~200 mg) are large enough to be homogeneous and representative of the average $^3He_{ET}$ concentration of their belonging stratigraphic layers. Hence, we compute for each sample a weighted average $^3He_{ET}$ concentration based on the uncertainty weighted mean of all aliquots (Fig. 7; Supp. Table 4). For the Bajocian samples, average $^3He_{ET}$ concentrations in the non-carbonate fractions are

(0.95±0.20) × 10^6 at/g and (1.20±0.34) × 10^6 at/g in the marl and limestone samples, respectively (Fig. 7). The Valanginian samples display slightly higher $^3He_{ET}$ concentrations in the non-carbonate fractions: (1.70±0.30) × 10^6 at/g and (1.54±0.12) × 10^6 at/g in the marl and limestone, respectively (Fig. 6).

Hence, $^3He_{ET}$ concentrations of the silici-clastic fractions are similar, within uncertainties, between marl and limestones in both Bajocian and Valanginian samples. In other words, $^3He_{ET}$ measured in the non-carbonate fraction is not correlated with the $CaCO_3$ content of the sample (Fig. 7A).

Mean $^3He_{ET}$ concentrations in Bajocian total bulk sediments (i.e., when the $CaCO_3$ fraction is considered) are respectively (0.28±0.14) × 10^6 at/g and (0.41±0.11) × 10^6 at/g in limestones and marls. The $^3He_{ET}$ concentrations in Valanginian total bulk sediments are (0.31±0.06) × 10^6 at/g in limestones and (0.74±0.14) × 10^6 at/g in marls. The $CaCO_3$ contents are hence negatively correlated with $^3He_{ET}$ total concentrations, both in the Bajocian and Valanginian samples (Fig. 7B).

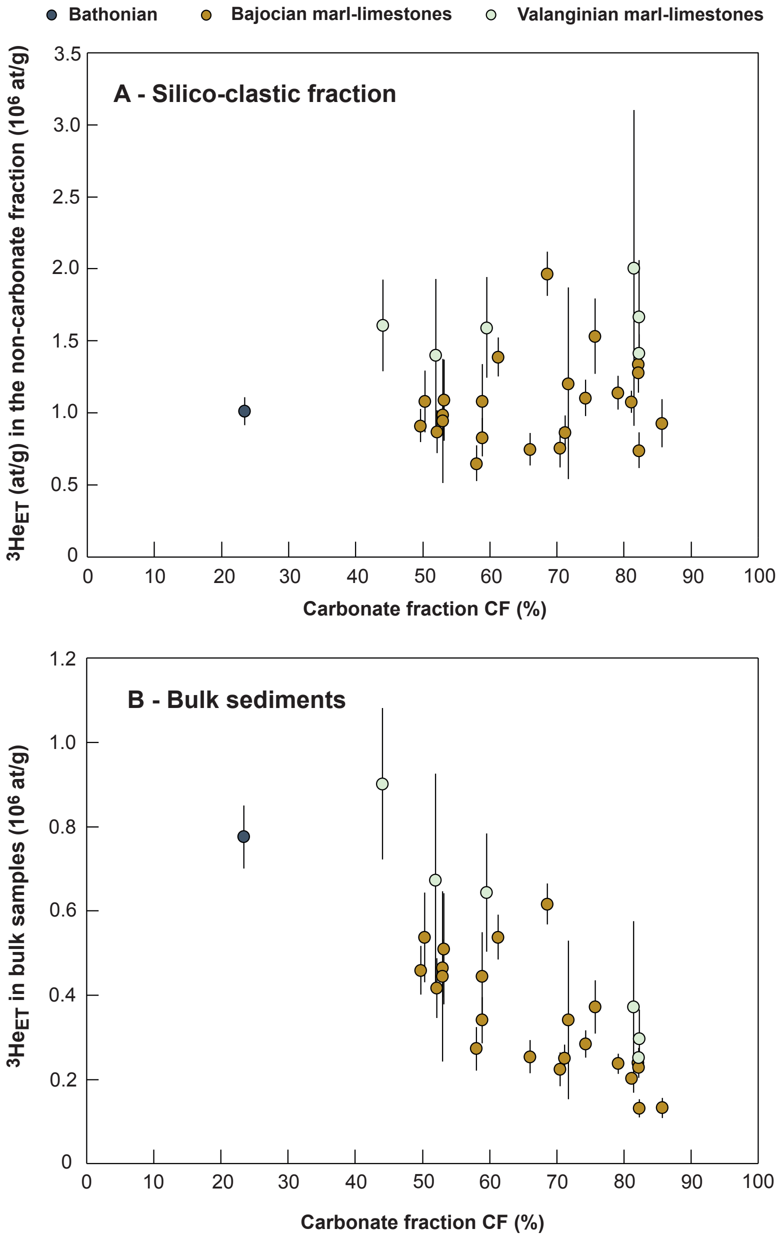

Figure 7 – $^3He_{ET}$ vs $CaCO_3$ proportion (wt%) in A) the silici-clastic (non-carbonate) fraction and B) in the bulk sediments. Multiple aliquots were weighted average to yield a mean concentration for each sample.

4.3 - $^3He_{ET}$-derived sedimentation rates

Applying equations 2) to 4) and a constant $^3He_{ET}$ flux of 100 pcc.cm^{-2}.Ma^{-1} (derived from (Farley et al, 2012) the obtained $^3He_{ET}$ concentrations yield silici-clastic sedimentation rates ranging between 5.5±0.4 and 16.8±3.2 m.Ma^{-1} for the Bajocian samples, and between 5.2±2.8 m/Ma and 8.0±3.0 m/Ma for the Valanginian samples. Total sedimentation rates range from 17.4±1.4 m/Ma to 78±13 m/Ma for the Bajocian section and from 12.7±2.5 m/Ma to 41.0±3.8 m/Ma for the Valanginian section (Supp. Table 4, Figs. 4,5 and 8). Total sedimentation rates show a non-linear positive correlation with the $CaCO_3$ contents of the analyzed strata (Fig. 8). Such a relationship is typical of carbonate-dominated systems fed by constant detrital fluxes (Fig. 7-3 in Ricken 1993).

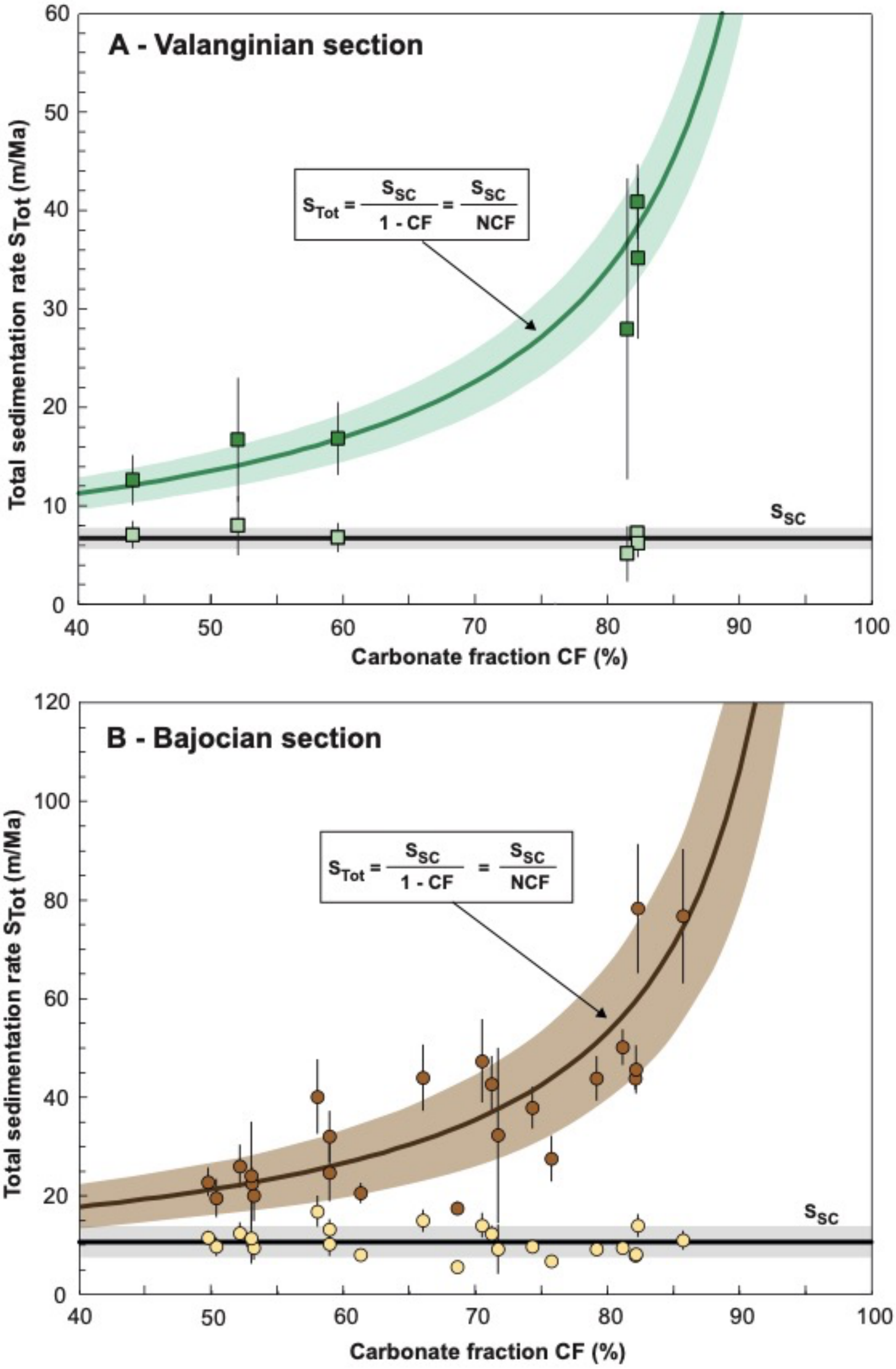

Fig. 8 – $^3He_{ET}$ derived silici-clastic (S_{SC}) and total sedimentation rates (S_{Tot}) plotted against the carbonate fraction ($CaCO_3$ proportion in wt%) in the analyzed dataset. Circles are individual data points while curves are computed as follow: S_{SC} horizontal

line is the mean of all data point, while the S_{Tot} curve is calculated using equation (3) and this mean S_{SC} value: $S_{Tot}=S_{SC}/NCF$.

4.4 - Rock-Eval pyrolysis

The Rock-Eval results are presented in Supp. Table 5. The TOC values are similar in both successions: 0.11-0.5 wt.% in the Bajocian samples (Fig. 4) and 0.10-0.44 wt.% in the Valanginian samples (Fig. 5). The T_{max} values are much higher in the Bajocian samples than in the Valanginian samples (mean 502°C versus 436°C), suggesting that the kerogen in the oldest samples is thermally overmature, whereas that of the youngest samples is immature to slightly mature. It should be noted, however, that the Bajocian samples record very low S2 values (<0.2 mg HC/g), characteristics of overmature samples, that often produces multimodal S2 peaks and hence erroneous T_{max} values (Yang and Horsfield 2020). The Rock-Eval pyrolysis values of the Bajocian samples should therefore be interpreted with caution in terms of thermal maturity and organic matter type. The Valanginian samples record higher S2 values (0.17 to 1.01 mg HC/g) that allow more reliable interpretation of the T_{max} and HI values. The Valanginian samples record higher HI values (27-229 mg HC/g TOC) than the Bajocian samples (22-72 mg HC/gTOC), whereas samples from both sites record comparable OI values (48-262 mg CO_2/gTOC). The Valanginian samples are hence dominated by type III kerogen (terrestrial and residual organic matter) with possibly little and variable amounts of type II kerogen (algal bacterial), whereas Bajocian samples contain highly altered, residual kerogen of type IV. These data indicate that the Valanginian samples likely experienced burial temperatures of 80°C.

4.5 – Abundance of calcareous nannofossils and their $CaCO_3$ contribution

The nannofossils results are reported in Supp. Table 6. Calcareous nannofossil absolute abundances range between 9.6×10^6 and 2.2×10^8 nannofossil/g in the Bajocian samples, with the exception of three samples whose nannofossil content was below the detection limit of the method. The carbonate-rich beds tend to have lower calcareous nannofossil absolute and relative abundances than marlstones intervals (Fig. 9D). The absolute abundances in the Valanginian samples range between 6.2×10^7 and 3.8×10^8 nannofossil/g, but, contrary to the

Bajocian samples, this section does not show a clear correlation with the $CaCO_3$ contents of the sediments (Fig. 9D).

Calcareous nannofossil calcium carbonate contribution to the bulk rock is ranging between 0 wt% and 2.2 wt% in the Bajocian section (Fig. 4) and between 1.9 wt% and 6.1 wt% in the Valanginian section (Fig. 5). The relative abundance of nannofossils is lower in the base of the Bajocian section and tend to increase in the upper part, but this nannofossil content seems similar, within uncertainties, between limestones and marlstones. In the Valanginian, however, the marlstones display slightly higher $CaCO_{3Nanno}$ values than limestones. Nevertheless, in both sections, the values are very low (<10%), implying that nannofossils are not the main source of $CaCO_3$ in these samples (Figs. 4 and 5).

5. Discussion

5.1 - Accuracy of the $^3He_{ET}$-derived sedimentation rates

5.1.1) Representativity of a 200 mg aliquot – number of analyzed IDPs.

Multi-aliquots (n = 2 to 4) $^3He_{ET}$ analyses from 18 different samples yield interaliquot weighted standard deviations of ~30%. Experimental observations indicate that the majority of the $^3He_{ET}$ signal preserved in oceanic sediments resides in IDPs smaller than 10 μm diameter, with a mode between 2 and 10 μm (McGee and Mukhopadhyay 2013; Mukhopadhyay and Farley 2006). Given that the $^3He_{ET}$ concentrations in IDPs is ~3×10^{14} at/g (Kehm et al., 2006), an IDP of 5 μm diameter bears ~4×10^4 at of $^3He_{ET}$, assuming these particles are spherical and have a density of 2 g/cm^3 (Kehm et al., 2006). Hence, the average $^3He_{ET}$ amount of 2×10^5 at of $^3He_{ET}$ measured in the silicate fraction of a ~0.2 g aliquot is carried on average by ~6 IDPs of 5 μm. Assuming that the number of IDPs present in one sample follows a Poisson distribution, we can compute the theoretical uncertainty arising from this interaliquots variability as $\sigma = 1/\sqrt{N}$, (N being the average number of IDPs present in one analyzed aliquot). With n = 5, σ ~40%, a value that is in good agreement with the observed interaliquots standard deviation of ~30% observed in this dataset. This good agreement confirms that the majority of the $^3He_{ET}$ signal relies on <10 μm IDPs rather than on micrometeorites larger than 50 μm (Stuart et al. 1999). Future studies may improve the representativity of analyzed samples and reduce the uncertainty. This can be done by using the same statistical approach, taking into account the silici-clastic sedimentation rate, to compute the number of IDPs present in a sample, and hence adjust the minimal sample mass required to be representative.

5.1.2) Validity of a constant $^3He_{ET}$ flux of 100 pcc.cm^{-2}.Ma^{-1}

There are only few paleorecords of $^3He_{ET}$ flux (F_{ET}) over pluri-million years timescales from well-dated sedimentary successions (McGee and Mukhopadhyay 2013), and even less for the Mesozoic period. For the Jurassic, (Chavrit et al., 2016) reported three measurements of $^3He_{ET}$ in the Toarcian of the Sancerre core (Paris Basin). The near-continuous record of F_{ET} between 100 and 30 Ma computed by Farley et al. 2012 from a stack of various datasets (Mukhopadhyay et al. 2001; Farley et al., 2012; 1998) shows a long-term average F_{ET} background of 100 pcc.cm^{-2}.Ma^{-1}. Although this reconstruction revealed transient increases at some periods, either caused by spike of $^3He_{ET}$ inputs, or by inaccuracy in the sediment age model, it however shows that these F_{ET} variations are very limited at timescale shorter than 100 ka. Given the likely short duration of the two successions analyzed here, we tentatively use a constant $^3He_{ET}$ flux of 100 pcc.cm^{-2}.Ma^{-1} to compute sedimentation rates.

Heating experiments on fragments of meteorites in lab conditions reported by (Füri et al. 2013) show significant helium loss during the atmospheric entry of micrometeorites. However, the constant $^3He_{ET}$ flux of 100 pcc.cm^{-2}.Ma^{-1} calibrated by Farley et al (2012) was established using similar material to the one used in this study in terms of granulometry and sedimentological conditions. Any potential atmospheric loss is hence cancelled off and already accounted for in the 100 pcc.cm^{-2}.Ma^{-1} flux and we thus assume this effect to have a negligible impact on the $^3He_{ET}$-based reconstructed sedimentation rates.

5.1.3) Thermal history of the sediments and preservation of the $^3He_{ET}$ signal

Post depositional alteration of the initial $^3He_{ET}$ burial may have occurred, either by thermal diffusion (Mukhopadhyay and Farley 2006) or weathering. According to the Rock-Eval pyrolysis data, the Bajocian samples are overmature, while the Valanginian samples are immature to slightly mature and likely experienced burial temperatures of 80°C. This temperature range is in rather good agreement with the thermochronological data from the nearby Oligocene sediments of the Vélodrome site, indicating that the southern part of the Barles half-window reached 120°C between 12 and 6 Ma (Schwartz et al. 2017), as a result of the emplacement of the ~3 km-thick Digne thrust sheet. The higher maturity of Bajocian samples indicated by the Rock-Eval pyrolysis could be partially due to lateral variations in the thickness of the Digne thrust. However, this differential heating more surely results from the Mesozoic and Cenozoic pile that buried the Bajocian below at least 4 km (120°C assuming a 30°C/km geothermal gradient), before deformation and exhumation started at the Oligocene (34 Ma) (Ford et al. 2006).

One may question whether this burial heating has led to partial loss of the initial $^3He_{ET}$ signal. Using thermal diffusion modeling based on experimental data from sea floor IDPs-rich sediments, (Mukhopadhyay and Farley 2006) suggested that temperatures above 100°C during 5 Ma are sufficient to completely (>99%) release the initial $^3He_{ET}$ signal from IDPs. However, these IDPs diffusion parameters were established by heating the samples between 200°C and 1400°C and extrapolated below 200°C using an Arrhenius relationship assuming a single diffusion domain, a simplification that may lead to inaccuracies (Delon et al. 2018). Hence, uncertainties about ^3He diffusions in IDPs hamper to precisely compute and constrain the amount of $^3He_{ET}$ that may have been lost during the burial history of these Bajocian and Valanginian sediments. However, some key observations indicate that the $^3He_{ET}$ loss has been limited (negligible) in these sediments since their deposition, and that thermal loss does not constitute a major source of inaccuracy in this dataset:

First, the $^3He/^4He$ ratios measured in our dataset are significantly higher than the crustal ($^3He/^4He$) endmember, an observation that strongly supports the presence of a $^3He_{ET}$ signal in the samples (Fig. 6). Second, there is a good agreement between the mean $^3He_{ET}$-derived sedimentation rates and those established from biostratigraphy (see next section 5.1.4). If significant post-depositional $^3He_{ET}$ loss had occurred, the $^3He_{ET}$-based sedimentation rates would have been higher than those based on biostratigraphy.

5.1.4) Agreement between the $^3He_{ET}$-derived sedimentation rates and the long-term rates based on the stratigraphic timescale

Comparing the average sedimentation rates determined by $^3He_{ET}$ with those obtained from biostratigraphy on million-year timescales provides clues on the accuracy of the $^3He_{ET}$ "sedimentometer" and the preservation of this signal. The average (± average of 1σ uncertainties) of our $^3He_{ET}$-based total sedimentation rates are 36±6 $m.Ma^{-1}$ and 25±7 $m.Ma^{-1}$ for the Bajocian and the Valanginian samples, respectively (Figs. 4 and 5). Using the GTS2020 biostratigraphic timescale (Gradstein et al. 2020), the average local sedimentation rates for these two stages are 37 $m.Ma^{-1}$ and 29 $m.Ma^{-1}$, respectively. This good agreement suggests that the $^3He_{ET}$ flux during the Middle Jurassic and Early Cretaceous times did not depart substantially from the Late Cretaceous flux of 100 pcc.cm^{-2}.Ma^{-1} computed by (Farley et al 2012). This observation also suggests that the initial extraterrestrial ^{3}He signal contained in the IDPs have been preserved in the sediments, even after their burial and heating above 80°C. The sedimentation rate computed from the single $^3He_{ET}$ measurements from the Bathonian-Oxfordian black shales is 15±1 m.Ma^{-1}, whereas the biostratigraphic constraints yield a higher mean deposition rate of 60 m.Ma^{-1}. Given that only one sample was analyzed in the Bathonian black shales, this apparent discrepancy is difficult to interpret. However, if helium loss had occurred, the $^3He_{ET}$ sedimentometer would have on the contrary yielded higher sedimentation rate that the biostratigraphic estimate.

5.2 - Control of the sedimentation rates at the orbital time scale

The $^3He_{ET}$-derived sedimentation rates indicate constant (within uncertainties) silici-clastic fluxes in both the Bajocian and Valanginian samples (Figs. 3, 4 and 7). On the contrary, sedimentation rates correlate positively with $CaCO_3$ contents in both sections (Figs. 3, 4 and 7). This observation indicates that astronomically driven environmental changes led to strong changes in $CaCO_3$ deposition fluxes, leading to variable dilution of the overall constant terrigenous silici clastic and the $^3He_{ET}$ inputs (Fig. 9A and C). Moreover, both the TOC (%) and the SiO_2 fraction - a proxy of the silici-clastic abundance - show a strong negative correlation with the $CaCO_3$ proportion (Fig. 9), supporting a similar mechanism of increasing dilution by higher $CaCO_3$ fluxes. The same dilution mechanism is also reflected by the decrease in the nannofossil $CaCO_3$ contribution with increasing total $CaCO_3$, in the case of the Bajocian samples (Fig. 9D), despite it is not the case for the Valanginian section (Fig. 9D).

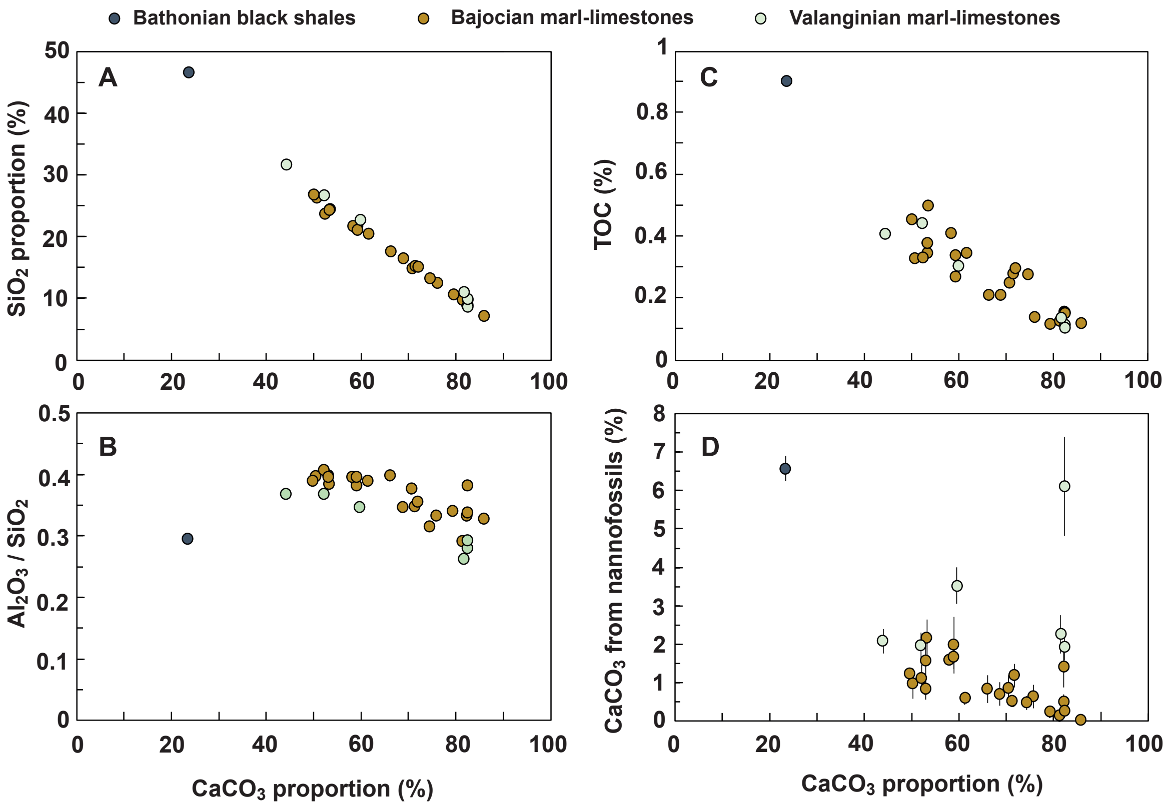

Figure 9 – Plots of several proxies against the $CaCO_3$ proportion (wt%): A) SiO_2 proportion (wt%) – a proxy of the silici-clastic fraction, B) Al_2O_3/SiO_2 – a proxy of the clays/quartz ratio, C) Total organic carbon (TOC, wt%), D) $CaCO_3$ proportion from nannofossils (wt%)

$^3He_{ET}$-based sedimentation rates may tentatively be used to constrain the durations of a single limestone-marl duplet by building high resolution age models (Figs. 4 and 5): in the case of the Bajocian section, our data yield durations of ~38 ka (BAJ 1-2 duplet), ~38 ka (BAJ 3-4 duplet) and ~29 ka (BAJ 5-6 duplet) (Fig. 4). Interestingly, the lithology of the Bajocian section (Fig. 3) suggests that marl interbeds contain another cycle, which would be consistent with the obliquity/precession hierarchy.

The Valanginian limestone-marl duplet correspond to a total duration of ~37 ka (Fig. 5). Those periods are close to the typical period of obliquity forcing (that was ~38 ka during the Cretaceous, Berger et al 1992), which has been independently identified by cyclostratigraphic studies of Cretaceous marl-limestone alternations in Southern France (Martinez et al. 2013; 2015). This agreement should be taken with caution since $^3He_{ET}$

sedimentation rates are based on a $^3He_{ET}$ flux derived from the Cretaceous (Farley et al., 2012), and not specifically calibrated for the Valanginian or the Bajocian. These durations could hence be revised upward or downward in the future using $^3He_{ET}$ flux from independently well-dated sections of the same area and age. A second limitation of our dataset is that it only covers few marl-limestone duplets and is hence too small to provide a statistically significant spectral analysis of cyclicity. The strength of the $^3He_{ET}$ approach is to be complementary of classical spectral approaches in cyclostratigraphy (e.g. Westerhold et al. 2020; De Vleeschouwer et al. 2013), by bringing higher-resolution internal time constraints at the scale of a marl-limestone cycle. Our data indeed show for the first time that, in this Southern France Mesozoic setting, limestone strata are characterized by a "time dilatation" due to larger sedimentation rates, hence corresponding to much shorter duration than the deposition of marl strata (Figs. 4 and 5). Since variations in the $^3He_{ET}$ flux are likely limited at timescales shorter than 100 ka (McGee and Mukhopadhyay 2013), these relative changes in sedimentation can be interpreted with confidence.

5.3 – A steady silici-clastic flux despite variable weathering conditions at the orbital timescale?

In comparable settings, cyclic variations in clay mineralogy between marl and limestones bed have been identified and interpreted as evidences for precipitation-driven changes in weathering at the orbital timescale (e.g. Martinez et al. 2015; Deconinck et al. 2003). Our results based on the $^3He_{ET}$ sedimentometer indicate constant terrigenous fluxes in marl and limestones beds at the orbital timescale (Figs. 4, 5, 8).

This contradiction may however be more apparent than real, for instance if orbitally-driven weathering fluctuations were not accompanied by significant changes in the efficiency of physical erosion rates over the continents. It is also possible that reduced fluvial clay-rich inputs were compensated by higher eolian quartz-rich input during arid phases (and vice and versa during humid phases). Such a compensatory mechanism is supported by the partial correlation between the Al_2O_3/SiO_2 ratio and the granulometric variations of the silici-clastic fraction (D_{50}) (Figs. 4 and 5). Accordingly, marl deposition would have occurred during wet phases with higher clay inputs, and limestone deposition during drier periods with higher eoalian blown quartz propotions. Overall, this hypothetical relationship between changes in humidity and $CaCO_3$ contents agrees with that inferred from clay mineral data in comparable settings (Moiroud et al. 2012). More data should be obtained from various paleolatitudes and chronozones to better characterize variations in the nature and the flux of the silici-clastic components.

5.4 – Causes of the $CaCO_3$ flux variability at the orbital timescale

The main implication of our highly resolved $^3He_{ET}$ dataset is that the studied marl-limestone cycles resulted from cyclic and large changes in $CaCO_3$ mud inputs driven by insolation variations at the orbital timescale (Fig. 4, 5 and 8). This observation is important for improving our understanding of the orbitally-driven sedimentary mechanisms leading to marl-limestone alternations (Ricken 1993; Einsele et al. 1982). A quite straightforward mechanism is a cyclic climate control on the carbonate factory (Reboulet et al. 2003). Our microfossil data show that this variability is not controlled by changes in pelagic $CaCO_3$ production from calcareous nannoplankton (Figs. 3, 4 and 8), in line with previous studies of Bajocian (Sucheras-Marx et al. 2013) and Valanginian (Gréselle et al. 2011) strata from the Vocontian Basin. The main source of variability could therefore be changes in the flux of allochtonous, platform-derived $CaCO_3$ mud (e.g. Reboulet et al. 2003; Gréselle et al. 2011). Previous studies have identified the Provence carbonate platform as the most likely source of this mud for the Valanginian interval (Reboulet et al. 2003) (Fig. 2). Such a modulation of the micritic $CaCO_3$ accumulation rate could either result from variations of primary production in the nearby "carbonate factory" platforms (Schlager 2005), or changes in efficiency of the lateral transfer of $CaCO_3$ (e.g. Andrieu et al. 2022). Environmental conditions (temperature, salinity, water transparency) may indeed favor or inhibit biologically induced $CaCO_3$ production (Michel et al, 2018) or its preservation in the water column (Sulpis et al. 2021). As mentioned above (section 5.3), higher carbonate production may have occurred during drier intervals with lower clay input, promoting carbonate platform growth through water transparency. Further identification of the specific involved environmental factors would be largely speculative given the lack of constraints about the ecology and nature of the main micrite producers. Given the ramp-morphology of the Provence platform, changes in $CaCO_3$ fluxes could alternatively or additionally imply rhythmic distal-to-proximal migration of facies belts related to sea level changes (Andrieu et al. 2022). Such rhythmic sea level fluctuations at the orbital timescale would point to climatically driven eustasy (Sames et al. 2016; Ray et al. 2019). Aquifer- and thermal-eustasy have been repeatedly suggested as drivers of sea-level changes during Mesozoic greenhouse climates, but require extreme climatic changes that seem incompatible with data (Ray et al. 2019). By contrast, eustatic changes linked to the demise/growth of ice sheets is consistent with oxygen isotope data and the abundance of glendonites at high paleolatitudes, which place the Bajocian as one of the coolest periods of the Jurassic (Dera et al. 2011). The presence of Bajocian icesheets, in the absence of absolute temperature estimates and definitive sedimentological evidence, however remains speculative. The Valanginian has also been suggested as being a relatively cool climate period (e.g. Cavalheiro et al. 2021) and modeling results show that the presence of a proto ice cap in Antarctica was possible during several periods of the Cretaceous greenhouse (Ladant and Donnadieu 2016). Variations of ice sheet volume in Antarctica had the potential to induce sea level fluctuations of few meters to several tens of meters during the Mesozoic (Donnadieu et al. 2011), which would have led to cyclic starvation of the platform $CaCO_3$ production or change in $CaCO_3$ export efficiency.

5.5 – Are variations of $CaCO_3$ also dominant at longer time scale?

The pioneering work of Ricken (1993) revealed that carbonate-dominated successions deposited over long interval (> 1 Ma) in reefal, hemipelagic and deep-sea settings are characterized by a non-linear positive relationship between total sedimentation rates and $CaCO_3$ content (Fig. 7-3 in Ricken 1993). This relationship implies that the $CaCO_3$ deposition flux is the main source of temporal variability in such carbonate-rich systems. Our new ^{3}HeET data show that this relationship is also valid on much shorter orbital timescale (< 10 ka) in hemipelagic settings (Fig. 8). A comparable $CaCO_3$ dilution mechanism may also dominate deep-sea carbonate-rich rhythmic sequences of Mesozoic and Cenozoic age. Available ^{3}He records of the Paleocene-Eocene transition (Farley and Eltgroth 2003; Murphy et al. 2010), for instance, indicate rather constant $^3He_{ET}$ concentrations in the non-carbonate fraction in carbonate-rich, deep-sea strata recovered at ODP sites 690 (Weddell Sea, Southern Ocean) and 1266 (Walvis Ridge, Southern Atlantic). These data also suggest that variable carbonate input (through dissolution or variable surface export) was the main controlling mechanism of sedimentation rates in deep-sea carbonate-rich strata. Such a “fractal” behavior suggests the existence of a robust and temporally invariant driving mechanism in many carbonate-rich, marl-limestone rhythmic depositional sequences. However, a dominant control of carbonate input on rhythmic sedimentation is certainly not universal. The data compiled by Ricken (1993) show that sedimentation rates are largely controlled by siliciclastic input near active margins with high rates of clastic input (Ricken 1993). Notable examples include upper Cretaceous successions deposited on the western margin of the Western Interior Seaway (USA), where some studies found that the main driver of the marl-limestone alternations was silici-clastic fluctuations (e.g. Locklair and Sageman 2008). In such cases, lateral or temporal changes in clastic input may exert, through variable dilution, a strong influence on organic carbon contents (Ricken 1993). A similar dilution of organic carbon (by carbonate input) is clearly apparent in our dataset (Figs. 3, 4 and 8). It thus remains to investigate to which extend recurrent intervals of higher organic contents recorded in many Mesozoic sequences systematically reflect periods of lower clastic or carbonate input. The application of the $^{3}He_{ET}$ approach used herein could therefore bring valuable clues to better identify the fundamental drivers of such episodes of organic enrichment. The ^{3}He methodology notably holds potential to reconstruct sedimentary fluxes with a millennial resolution across episodes of rapid and global biogeochemical perturbations, such as the Oceanic Anoxic Event 2 at the Cenomanian-Turonian transition.

Concluding remarks

- Our high resolution $^{3}He_{ET}$ records from two pilot marl-limestone sections of the Bajocian (3.4 m) and the Valanginian (0.9 m) of Haute-Provence (Barles) show that the silici-clastic flux was constant through these marl limestone alternations. Nannofossil abundances indicate that the main drivers of the total sedimentation rates are flux changes in platform-derived $CaCO_3$ mud, and not the pelagic productivity.

- Total sedimentation rates derived from $^{3}He_{ET}$ at the "orbital scale" agree with mean bio-cyclostratigraphic estimates, supporting the use of $^{3}He_{ET}$ as a reliable high resolution sedimentometer, even in Middle Jurassic-Lower Cretaceous deposits.

- Previous work suggested variable detrital input as the dominant controlling factor of sedimentation rates at both orbital- and Ma-timescale in some Upper Cretaceous hemipelagic strata of the Western Interior Seaway deposited closer to active margins (e.g., Ricken, 1993; Locklair and Sageman, 2008). Hence, applying the $^{3}He_{ET}$ tool to these other settings will be a key to test whether $CaCO_3$ variability was a ubiquitous driver of Mesozoic marl limestone alternations.

Acknowledgments

The inspiration of this exploratory work is rooted in a question that professor Bernard Charoy asked to PHB 20 years ago during a sedimentology exam at ENSG. Myette Guiomar, Didier Bert and the "*Réserve Naturelle Géologique de Haute Provence*" are thanked for field authorizations. PHB acknowledges Bouchaïb Tibari and Laurent Zimmermann for their support during noble gas analysis at CRPG. BSM thanks Sandrine Conrod for micropaleontology lab management and teaching TM the random-settling protocol. BSM also thanks Yves Gally for microscopy lab management and software development for TM internship in spring 2021. This manuscript is a contribution to Climate scientific team at CEREGE (BSM).

Authors contribution

PHB, BSM and GS designed the study, interpreted the data, performed the calculations and wrote the initial draft of the article. PHB and JD made the field sampling. PHB built the figures. TM performed the nannofossils counting under the supervision of BSM. TA performed the Rock-Eval analysis. BG participated in calculations and data interpretation. All authors edited the paper.

REFERENCES

Abell, Jordan T., Gisela Winckler, Robert F. Anderson, and Timothy D. Herbert. 2021. "Poleward and Weakened Westerlies during Pliocene Warmth." *Nature* 589 (7840): 70–75. https://doi.org/10.1038/s41586-020-03062-1.

Agard, P., and M. Lemoine. 2005. "Faces of the Alps: Structural and Geodynamic Evolution." *Commission de La Carte Géologique Du Monde*, 50.

Andrews, J. N., and R. L. F. Kay. 1982. "Natural Production of Tritium in Permeable Rocks." *Nature* 298 (5872): 361–63. https://doi.org/10.1038/298361a0.

Andrews, J.N. 1985. "The Isotopic Composition of Radiogenic Helium and Its Use to Study Groundwater Movement in Confined Aquifers." *Chemical Geology* 49 (1–3): 339–51. https://doi.org/10.1016/0009-2541(85)90166-4.

Andrieu, Simon, François-Nicolas Krencker, and Stéphane Bodin. 2022. "Anatomy of a Platform Margin during a Carbonate Factory Collapse: Implications for the Sedimentary Record and Sequence Stratigraphic Interpretation of Poisoning Events." *Journal of the Geological Society* 179 (6): jgs2022-005. https://doi.org/10.1144/jgs2022-005.

Beaufort, Luc. 1991. "Adaptation of the Random Settling Method for Quantitative Studies of Calcareous Nannofossils." *Micropaleontology* 37 (4): 415. https://doi.org/10.2307/1485914.

Beaufort, Luc, Nicolas Barbarin, and Yves Gally. 2014. "Optical Measurements to Determine the Thickness of Calcite Crystals and the Mass of Thin Carbonate Particles Such as Coccoliths." *Nature Protocols* 9 (3): 633–42. https://doi.org/10.1038/nprot.2014.028.

Behar, F., V. Beaumont, and H. L. De B. Penteado. 2001. "Rock-Eval 6 Technology: Performances and Developments." *Oil & Gas Science and Technology* 56 (2): 111–34. https://doi.org/10.2516/ogst:2001013.

Berger, A., M. F. Loutre, and J. Laskar. 1992. "Stability of the Astronomical Frequencies Over the Earth's History for Paleoclimate Studies." *Science* 255 (5044): 560–66. https://doi.org/10.1126/science.255.5044.560.

Berger, André, Marie-France Loutre, and Christian Tricot. 1993. "Insolation and Earth's Orbital Periods." *Journal of Geophysical Research* 98 (D6): 10341. https://doi.org/10.1029/93JD00222.

Blard, P.-H. 2021. “Cosmogenic 3He in Terrestrial Rocks: A Review.” *Chemical Geology* 586 (December): 120543. https://doi.org/10.1016/j.chemgeo.2021.120543.

Blard, P.-H., G. Balco, P. G. Burnard, K. A. Farley, C. R. Fenton, R. Friedrich, A. J T Jull, et al. 2015. “An Inter-Laboratory Comparison of Cosmogenic 3He and Radiogenic 4He in the CRONUS-P Pyroxene Standard.” *Quaternary Geochronology* 26: 11–19. https://doi.org/10.1016/j.quageo.2014.08.004.

Carignan, Jean, Pascal Hild, Guy Mevelle, Jacques Morel, and Delphine Yeghicheyan. 2001. “Routine Analyses of Trace Elements in Geological Samples Using Flow Injection and Low Pressure On-Line Liquid Chromatography Coupled to ICP-MS: A Study of Geochemical Reference Materials BR, DR-N, UB-N, AN-G and GH.” *Geostandards and Geoanalytical Research* 25 (2–3): 187–98. https://doi.org/10.1111/j.1751-908X.2001.tb00595.x.

Cariou, E., and P. Hantzpergue. 1997. *Biostratigraphie Du Jurassique Ouest-Européen et Méditerranéen – Zonations Parallèles et Distribution Des Invertébrés et Microfossiles*. Bulletin Des Centres de Recherches Elf Exploration-Production. Paris.

Cavalheiro, Liyenne, Thomas Wagner, Sebastian Steinig, Cinzia Bottini, Wolf Dummann, Onoriode Esegbue, Gabriele Gambacorta, et al. 2021. “Impact of Global Cooling on Early Cretaceous High PCO2 World during the Weissert Event.” *Nature Communications* 12 (1): 5411. https://doi.org/10.1038/s41467-021-25706-0.

Charbonnier, Guillaume, Stéphanie Duchamp-Alphonse, Thierry Adatte, Karl B. Föllmi, Jorge E. Spangenberg, Silvia Gardin, Bruno Galbrun, and Christophe Colin. 2016. “Eccentricity Paced Monsoon-like System along the Northwestern Tethyan Margin during the Valanginian (Early Cretaceous): New Insights from Detrital and Nutrient Fluxes into the Vocontian Basin (SE France).” *Palaeogeography, Palaeoclimatology, Palaeoecology* 443 (February): 145–55. https://doi.org/10.1016/j.palaeo.2015.11.027.

Chavrit, Déborah, Manuel A. Moreira, and Frédéric Moynier. 2016. “Estimation of the Extraterrestrial 3 He and 20 Ne Fluxes on Earth from He and Ne Systematics in Marine Sediments.” *Earth and Planetary Science Letters* 436 (February): 10–18. https://doi.org/10.1016/j.epsl.2015.12.030.

De Vleeschouwer, David, Michał Rakociński, Grzegorz Racki, David P.G. Bond, Katarzyna Sobień, and Philippe Claeys. 2013. “The Astronomical Rhythm of Late-Devonian Climate Change (Kowala Section, Holy Cross Mountains, Poland).” *Earth and Planetary Science Letters* 365 (March): 25–37. https://doi.org/10.1016/j.epsl.2013.01.016.

Deconinck, Jean-François, Stephen P. Hesselbo, Nicolas Debuisser, Olivier Averbuch, François Baudin, and Julian Bessa. 2003. “Environmental Controls on Clay Mineralogy of an Early Jurassic Mudrock (Blue Lias Formation, Southern England).” *International Journal of Earth Sciences* 92 (2): 255–66. https://doi.org/10.1007/s00531-003-0318-y.

Delon, Rémi, Sylvie Demouchy, Yves Marrocchi, Mohammed Ali Bouhifd, Fabrice Barou, Patrick Cordier, Ahmed Addad, and Pete G. Burnard. 2018. “Helium Incorporation and Diffusion in Polycrystalline Olivine.” *Chemical Geology* 488 (June): 105–24. https://doi.org/10.1016/j.chemgeo.2018.04.013.

Dera, Guillaume, Benjamin Brigaud, Fabrice Monna, Rémi Laffont, Emmanuelle Pucéat, Jean-François Deconinck, Pierre Pellenard, Michael M. Joachimski, and Christophe Durlet. 2011. “Climatic Ups and Downs in a Disturbed Jurassic World.” *Geology* 39 (3): 215–18. https://doi.org/10.1130/G31579.1.

Donnadieu, Yannick, Gilles Dromart, Yves Goddéris, Emmanuelle Pucéat, Benjamin Brigaud, Guillaume Dera, Christophe Dumas, and Nicolas Olivier. 2011. “A Mechanism for Brief Glacial Episodes in the Mesozoic Greenhouse: A MECHANISM FOR BRIEF GLACIAL EPISODES.” *Paleoceanography* 26 (3): n/a-n/a. https://doi.org/10.1029/2010PA002100.

Einsele, Gerhard, Adolf Seilacher, and Sonderforschungsbereich Paläontologie unter

Besonderer Berücksichtigung der Palökologie, eds. 1982. *Cyclic and Event Stratification*. Berlin: Springer.

Espitalie, J., G. Deroo, and F. Marquis. 1985. "La Pyrolyse Rock-Eval et Ses Applications. Deuxième Partie." *Revue de l'Institut Français Du Pétrole* 40 (6): 755–84. https://doi.org/10.2516/ogst:1985045.

Farley, K. A. 1995. "Cenozoic Variations in the Flux of Interplanetary Dust Recorded By3He in a Deep-Sea Sediment." *Nature* 376 (6536): 153–56. https://doi.org/10.1038/376153a0.

Farley, K. A., A. Montanari, E. M. Shoemaker, and C. S. Shoemaker. 1998. "Geochemical Evidence for a Comet Shower in the Late Eocene." *Science* 280 (5367): 1250–53. https://doi.org/10.1126/science.280.5367.1250.

Farley, K.A., and S.F. Eltgroth. 2003. "An Alternative Age Model for the Paleocene–Eocene Thermal Maximum Using Extraterrestrial 3He." *Earth and Planetary Science Letters* 208 (3–4): 135–48. https://doi.org/10.1016/S0012-821X(03)00017-7.

Farley, K.A., A. Montanari, and R. Coccioni. 2012. "A Record of the Extraterrestrial 3He Flux through the Late Cretaceous." *Geochimica et Cosmochimica Acta* 84 (May): 314–28. https://doi.org/10.1016/j.gca.2012.01.015.

Farley, Kenneth A., David Vokrouhlický, William F. Bottke, and David Nesvorný. 2006. "A Late Miocene Dust Shower from the Break-up of an Asteroid in the Main Belt." *Nature* 439 (7074): 295–97. https://doi.org/10.1038/nature04391.

Ferreira, Jorge, Emanuela Mattioli, Baptiste Sucherás-Marx, Fabienne Giraud, Luis V. Duarte, Bernard Pittet, Guillaume Suan, Auguste Hassler, and Jorge E. Spangenberg. 2019. "Western Tethys Early and Middle Jurassic Calcareous Nannofossil Biostratigraphy." *Earth-Science Reviews* 197 (October): 102908. https://doi.org/10.1016/j.earscirev.2019.102908.

Ford, Mary, Stéphanie Duchêne, Dominique Gasquet, and Olivier Vanderhaeghe. 2006. "Two-Phase Orogenic Convergence in the External and Internal SW Alps." *Journal of the Geological Society* 163 (5): 815–26. https://doi.org/10.1144/0016-76492005-034.

Füri, Evelyn, Alice Aléon-Toppani, Bernard Marty, Guy Libourel, and Laurent Zimmermann. 2013. "Effects of Atmospheric Entry Heating on the Noble Gas and Nitrogen Content of Micrometeorites." *Earth and Planetary Science Letters* 377–378 (September): 1–12. https://doi.org/10.1016/j.epsl.2013.07.031.

Gilbert, G. K. 1895. "Sedimentary Measurement of Cretaceous Time." *The Journal of Geology* 3 (2): 121–27. https://doi.org/10.1086/607150.

Giraud, F., L. Beaufort, and P. Cotillon. 1995. "Astronomical Control of Carbonate Record in the Lower Cretaceous of the Vocontian Basin (SE France)." *Bulletin de La Société Géologique de France.* 166 (4): 409–21.

Graciansky, Pierre-Charles de, Jan Hardenbol, Thierry Jacquin, and Peter R. Vail. 1999. *Mesozoic and Cenozoic Sequence Stratigraphy of European Basins*. SEPM Society for Sedimentary Geology. https://doi.org/10.2110/pec.98.02.

Gradstein, F., J.G. Ogg, M.D. Schmitz, and G.M. Ogg. 2020. *Geologic Time Scale 2020.* Elsevier. https://doi.org/10.1016/C2020-1-02369-3.

Gréselle, Benjamin, Bernard Pittet, Emanuela Mattioli, Michael Joachimski, Nicolas Barbarin, Laurent Riquier, Stéphane Reboulet, and Emmanuelle Pucéat. 2011. "The Valanginian Isotope Event: A Complex Suite of Palaeoenvironmental Perturbations." *Palaeogeography, Palaeoclimatology, Palaeoecology* 306 (1–2): 41–57. https://doi.org/10.1016/j.palaeo.2011.03.027.

Haccart, D., B. Beaudoin, P. Gigot, and M. Jorda. 1989. "Notice Explicative de La Feuille de La Javie à 1/50 000." *BRGM Éditions, Service Géologique National* 918.

Huang, Chunju. 2018. "Astronomical Time Scale for the Mesozoic." In *Stratigraphy & Timescales*, 3:81–150. Elsevier. https://doi.org/10.1016/bs.sats.2018.08.005.

Ikeda, Masayuki, Maximilien Bôle, and Peter O. Baumgartner. 2016. "Orbital-Scale Changes in Redox Condition and Biogenic Silica/Detrital Fluxes of the Middle Jurassic Radiolarite in Tethys (Sogno, Lombardy, N-Italy): Possible Link with Glaciation?” *Palaeogeography, Palaeoclimatology, Palaeoecology* 457 (September): 247–57. https://doi.org/10.1016/j.palaeo.2016.06.009.

Jiang, Chunqing, Zhuoheng Chen, Denis Lavoie, Jeanne B. Percival, and Pavel Kabanov. 2017. “Mineral Carbon MinC(%) from Rock-Eval Analysis as a Reliable and Cost-Effective Measurement of Carbonate Contents in Shale Source and Reservoir Rocks.” *Marine and Petroleum Geology* 83 (May): 184–94. https://doi.org/10.1016/j.marpetgeo.2017.03.017.

Kehm, Karl, George J. Flynn, and Charles M. Hohenberg. 2006. “Noble Gas Space Exposure Ages of Individual Interplanetary Dust Particles.” *Meteoritics & Planetary Science* 41 (8): 1199–1217. https://doi.org/10.1111/j.1945-5100.2006.tb00516.x.

Ladant, Jean-Baptiste, and Yannick Donnadieu. 2016. “Palaeogeographic Regulation of Glacial Events during the Cretaceous Supergreenhouse.” *Nature Communications* 7 (1). https://doi.org/10.1038/ncomms12771.

Locklair, Robert E., and Bradley B. Sageman. 2008. “Cyclostratigraphy of the Upper Cretaceous Niobrara Formation, Western Interior, U.S.A.: A Coniacian–Santonian Orbital Timescale.” *Earth and Planetary Science Letters* 269 (3–4): 540–53. https://doi.org/10.1016/j.epsl.2008.03.021.

Mabry, Jennifer, Tefang Lan, Pete Burnard, and Bernard Marty. 2013. “High-Precision Helium Isotope Measurements in Air.” *J. Anal. At. Spectrom.* 28 (12): 1903–10. https://doi.org/10.1039/C3JA50155H.

Marcantonio, Franco, Robert F. Anderson, Martin Stute, Niraj Kumar, Peter Schlosser, and Alan Mix. 1996. “Extraterrestrial 3He as a Tracer of Marine Sediment Transport and Accumulation.” *Nature* 383 (6602): 705–7. https://doi.org/10.1038/383705a0.

Marcantonio, Franco, Sean Higgins, Robert F. Anderson, Martin Stute, Peter Schlosser, and E.Troy Rasbury. 1998. “Terrigenous Helium in Deep-Sea Sediments.” *Geochimica et Cosmochimica Acta* 62 (9): 1535–43. https://doi.org/10.1016/S0016-7037(98)00091-X.

Marcantonio, Franco, Niraj Kumar, Martin Stute, Robert F. Anderson, Michele A. Seidl, Peter Schlosser, and Alan Mix. 1995. “A Comparative Study of Accumulation Rates Derived by He and Th Isotope Analysis of Marine Sediments.” *Earth and Planetary Science Letters* 133 (3–4): 549–55. https://doi.org/10.1016/0012-821X(95)00079-R.

Marcantonio, Franco, Deborah J. Thomas, Stella Woodard, David McGee, and Gisela Winckler. 2009. “Extraterrestrial 3He in Paleocene Sediments from Shatsky Rise: Constraints on Sedimentation Rate Variability.” *Earth and Planetary Science Letters* 287 (1–2): 24–30. https://doi.org/10.1016/j.epsl.2009.07.029.

Martinez, Mathieu, Jean-François Deconinck, Pierre Pellenard, Stéphane Reboulet, and Laurent Riquier. 2013. “Astrochronology of the Valanginian Stage from Reference Sections (Vocontian Basin, France) and Palaeoenvironmental Implications for the Weissert Event.” *Palaeogeography, Palaeoclimatology, Palaeoecology* 376 (April): 91–102. https://doi.org/10.1016/j.palaeo.2013.02.021.

Martinez, Mathieu, Jean-François Deconinck, Pierre Pellenard, Laurent Riquier, Miguel Company, Stéphane Reboulet, and Mathieu Moiroud. 2015. “Astrochronology of the Valanginian–Hauterivian Stages (Early Cretaceous): Chronological Relationships between the Paraná–Etendeka Large Igneous Province and the Weissert and the Faraoni Events.” *Global and Planetary Change* 131 (August): 158–73. https://doi.org/10.1016/j.gloplacha.2015.06.001.

Matsuda, J., T. Matsumoto, H. Sumino, K. Nagao, J. Yamamoto, Y. Miura, I. Kaneoka, N. Takahata, and Y. Sano. 2002. “The 3He/4He Ratio of New Internal He Standard of Japan (HESJ).” *Geochemical Journal* 36 (2): 191–95. https://doi.org/10.2343/geochemj.36.191.

McGee, David, and Sujoy Mukhopadhyay. 2013. “Extraterrestrial He in Sediments: From

Recorder of Asteroid Collisions to Timekeeper of Global Environmental Changes.” In *The Noble Gases as Geochemical Tracers*, edited by Pete Burnard, 155–76. Advances in Isotope Geochemistry. Berlin, Heidelberg: Springer Berlin Heidelberg. https://doi.org/10.1007/978-3-642-28836-4_7.

Michel, Julien, Jean Borgomano, and John J.G. Reijmer. 2018. “Heterozoan Carbonates: When, Where and Why? A Synthesis on Parameters Controlling Carbonate Production and Occurrences.” *Earth-Science Reviews* 182 (July): 50–67. https://doi.org/10.1016/j.earscirev.2018.05.003.

Milankovitch, Milutin. 1941. “Kanon Der Erdbestrahlung Und Seine Anwendung Auf Das Eiszeitenproblem.” *Royal Serbian Academy Special Publication* 133: 1–633.

Moiroud, Mathieu, Mathieu Martinez, Jean-François Deconinck, Fabrice Monna, Pierre Pellenard, Laurent Riquier, and Miguel Company. 2012. “High-Resolution Clay Mineralogy as a Proxy for Orbital Tuning: Example of the Hauterivian–Barremian Transition in the Betic Cordillera (SE Spain).” *Sedimentary Geology* 282 (December): 336–46. https://doi.org/10.1016/j.sedgeo.2012.10.004.

Mount, J., and P. Ward. 1986. “Origin of Limestone/Marl Alterations in the Upper Maastrichtian of Zumaya, Spain.” *Journal of Sedimentary Research* 56 (2): 228–36. https://doi.org/10.1306/212F88C8-2B24-11D7-8648000102C1865D.

Mukhopadhyay, S., and K.a. Farley. 2006. “New Insights into the Carrier Phase(s) of Extraterrestrial 3He in Geologically Old Sediments.” *Geochimica et Cosmochimica Acta* 70 (19): 5061–73. https://doi.org/10.1016/j.gca.2006.06.1566.

Mukhopadhyay, S, K.A Farley, and A Montanari. 2001. “A 35 Myr Record of Helium in Pelagic Limestones from Italy: Implications for Interplanetary Dust Accretion from the Early Maastrichtian to the Middle Eocene.” *Geochimica et Cosmochimica Acta* 65 (4): 653–69. https://doi.org/10.1016/S0016-7037(00)00555-X.

Munnecke, A., H. Westphal, M. Elrick, and J. Reijmer. 2001. “The Mineralogical Composition of Precursor Sediments of Calcareous Rhythmites: A New Approach.” *International Journal of Earth Sciences* 90 (4): 795–812. https://doi.org/10.1007/s005310000137.

Murphy, B.H., K.A. Farley, and J.C. Zachos. 2010. “An Extraterrestrial 3He-Based Timescale for the Paleocene–Eocene Thermal Maximum (PETM) from Walvis Ridge, IODP Site 1266.” *Geochimica et Cosmochimica Acta* 74 (17): 5098–5108. https://doi.org/10.1016/j.gca.2010.03.039.

Nohl, Theresa, Manuel J. Steinbauer, Matthias Sinnesael, and Emilia Jarochowska. 2021. “Detecting Initial Aragonite and Calcite Variations in Limestone–Marl Alternations.” Edited by Cathy Hollis. *Sedimentology* 68 (7): 3102–15. https://doi.org/10.1111/sed.12885.

Olivero, D. 2003. “Early Jurassic to Late Cretaceous Evolution of Zoophycos in the French Subalpine Basin (Southeastern France).” *Palaeogeography, Palaeoclimatology, Palaeoecology* 192 (1–4): 59–78. https://doi.org/10.1016/S0031-0182(02)00679-X.

Peters. 1986. “Guidelines for Evaluating Petroleum Source Rock Using Programmed Pyrolysis.” *AAPG Bulletin* 70. https://doi.org/10.1306/94885688-1704-11D7-8645000102C1865D.

Pittet, Bernard, and Emanuela Mattioli. 2002. “The Carbonate Signal and Calcareous Nannofossil Distribution in an Upper Jurassic Section (Balingen-Tieringen, Late Oxfordian, Southern Germany).” *Palaeogeography, Palaeoclimatology, Palaeoecology* 179 (1–2): 71–96. https://doi.org/10.1016/S0031-0182(01)00409-6.

Protin, Marie, Pierre Henri Blard, Yves Marrocchi, and François Mathon. 2016. “Irreversible Adsorption of Atmospheric Helium on Olivine: A Lobster Pot Analogy.” *Geochimica et Cosmochimica Acta* 179: 76–88. https://doi.org/10.1016/j.gca.2016.01.032.

Ray, David C., Frans S.P. van Buchem, Graham Baines, Andrew Davies, Benjamin Gréselle, Michael D. Simmons, and Christopher Robson. 2019. “The Magnitude and Cause of Short-Term Eustatic Cretaceous Sea-Level Change: A Synthesis.” *Earth-Science Reviews* 197 (October): 102901. https://doi.org/10.1016/j.earscirev.2019.102901.

Reboulet, S, E Mattioli, B Pittet, F Baudin, D Olivero, and O Proux. 2003. “Ammonoid and Nannoplankton Abundance in Valanginian (Early Cretaceous) Limestone–Marl Successions from the Southeast France Basin: Carbonate Dilution or Productivity?” *Palaeogeography, Palaeoclimatology, Palaeoecology* 201 (1–2): 113–39. https://doi.org/10.1016/S0031-0182(03)00541-8.

Ricken, Werner. 1993. *Sedimentation as a Three-Component System - Organic Carbon, Carbonate, Noncarbonate*. Springer. Lecture Notes in Earth Sciences 51. Berlin, Heidelberg: Springer.

Sames, B., M. Wagreich, J.E. Wendler, B.U. Haq, C.P. Conrad, M.C. Melinte-Dobrinescu, X. Hu, et al. 2016. “Review: Short-Term Sea-Level Changes in a Greenhouse World — A View from the Cretaceous.” *Palaeogeography, Palaeoclimatology, Palaeoecology* 441 (January): 393–411. https://doi.org/10.1016/j.palaeo.2015.10.045.

Schlager, Wolfgang, ed. 2005. *Carbonate Sedimentology and Sequence Stratigraphy*. SEPM (Society for Sedimentary Geology). https://doi.org/10.2110/csp.05.08.

Schwartz, Stéphane, Cécile Gautheron, Laurence Audin, Thierry Dumont, Jérôme Nomade, Jocelyn Barbarand, Rosella Pinna-Jamme, and Peter van der Beek. 2017. “Foreland Exhumation Controlled by Crustal Thickening in the Western Alps.” *Geology* 45 (2): 139–42. https://doi.org/10.1130/G38561.1.

Stuart, F.M, P.J Harrop, S Knott, and G Turner. 1999. “Laser Extraction of Helium Isotopes from Antarctic Micrometeorites: Source of He and Implications for the Flux of Extraterrestrial 3He to Earth.” *Geochimica et Cosmochimica Acta* 63 (17): 2653–65. https://doi.org/10.1016/S0016-7037(99)00161-1.

Sucheras-Marx, Baptiste, Fabienne Giraud, Vincent Fernandez, Bernard Pittet, Christophe Lecuyer, Davide Olivero, and Emanuela Mattioli. 2013. “Duration of the Early Bajocian and the Associated δ^{13}C Positive Excursion Based on Cyclostratigraphy.” *Journal of the Geological Society* 170 (1): 107–18. https://doi.org/10.1144/jgs2011-133.

Sulpis, Olivier, Emil Jeansson, Ashley Dinauer, Siv K. Lauvset, and Jack J. Middelburg. 2021. “Calcium Carbonate Dissolution Patterns in the Ocean.” *Nature Geoscience* 14 (6): 423–28. https://doi.org/10.1038/s41561-021-00743-y.

Teng, F.-Z., W.F. McDonough, R.L. Rudnick, C. Dalpé, P.B. Tomascak, B.W. Chappell, and S. Gao. 2004. “Lithium Isotopic Composition and Concentration of the Upper Continental Crust.” *Geochimica et Cosmochimica Acta* 68 (20): 4167–78. https://doi.org/10.1016/j.gca.2004.03.031.

Van Os, B. J. H., L. J. Lourens, F. J. Hilgen, G. J. De Lange, and L. Beaufort. 1994. “The Formation of Pliocene Sapropels and Carbonate Cycles in the Mediterranean: Diagenesis, Dilution, and Productivity.” *Paleoceanography* 9 (4): 601–17. https://doi.org/10.1029/94PA00597.

Westerhold, Thomas, Norbert Marwan, Anna Joy Drury, Diederik Liebrand, Claudia Agnini, Eleni Anagnostou, James S. K. Barnet, et al. 2020. “An Astronomically Dated Record of Earth’s Climate and Its Predictability over the Last 66 Million Years.” *Science* 369 (6509): 1383–87. https://doi.org/10.1126/science.aba6853.

Woodard, Stella C., Deborah J. Thomas, Steve Hovan, Ursula Röhl, and Thomas Westerhold. 2011. “Evidence for Orbital Forcing of Dust Accumulation during the Early Paleogene Greenhouse: DUST ACCUMULATION DURING EARLY PALEOGENE.” *Geochemistry, Geophysics, Geosystems* 12 (2): n/a-n/a. https://doi.org/10.1029/2010GC003394.

Yang, Shengyu, and Brian Horsfield. 2020. “Critical Review of the Uncertainty of Tmax in Revealing the Thermal Maturity of Organic Matter in Sedimentary Rocks.” *International*

Journal of Coal Geology 225 (May): 103500. https://doi.org/10.1016/j.coal.2020.103500.

Zimmermann, Laurent, Guillaume Avice, Pierre-Henri Blard, Bernard Marty, Evelyn Füri, and Peter G. Burnard. 2018. “A New All-Metal Induction Furnace for Noble Gas Extraction.” *Chemical Geology* 480 (March): 86–92. https://doi.org/10.1016/j.chemgeo.2017.09.018.